Danish Meteorological Institute
Ministry for Climate and Energy

Danish Climate Centre Report 14-02

Presentation of the DMI-HIRHAM5 CORDEX AFRICA-44 simulation - v2, September, 2014

Cathrine Fox Maule

Colophone

Serial title:
Danish Climate Centre Report 14-02

Title:
Presentation of the DMI-HIRHAM5 CORDEX AFRICA-44 simulation - v2, September, 2014

Subtitle:
The DMI-HIRHAM5 CORDEX AFRICA simulation

Authors:
Cathrine Fox Maule

Other Contributers:
The front page picture is taken from NASA's "blue marble" image. Credit: NASA Goddard Space Flight Center Image by Reto Stöckli (land surface, shallow water, clouds). Enhancements by Robert Simmon (ocean color, compositing, 3D globes, animation). Data and technical support: MODIS Land Group; MODIS Science Data Support Team; MODIS Atmosphere Group; MODIS Ocean Group Additional data: USGS EROS Data Center (topography); USGS Terrestrial Remote Sensing Flagstaff Field Center (Antarctica); Defense Meteorological Satellite Program (city lights).

Responsible Institution:
Danish Meteorological Institute

Language:
English

Keywords:
CORDEX, DMI-HIRHAM5, Africa

Url:
www.dmi.dk/dmi/dkc14-02

ISSN:
1399-1957

ISBN:
978-87-7478-649-8 (online)

Version:
1

Website:
www.dmi.dk

Contents

1. Introduction

This report gives a short overview of the output of the CORDEX Africa, AFR-44, simulation by the regional climate model (RCM) DMI-HIRHAM5 (Christensen *et al.*, 2006), driven by the global climate model (GCM) ICHEC-EC-EARTH (Hazeleger *et al.*, 2012) version r3i1p1, by showing a series of maps of the model output. In Chapter 2 a short evaluation of the performance of DMI-HIRHAM5 over Africa is made by comparing the evaluation run, where DMI-HIRHAM5 has been driven by ECMWF's renalysis product ERA-interim, with observed temperature and precipitation. Chapter 3 presents some results from the GCM-RCM experiment ICHEC-EC-EARTH - DMI-HIRHAM5 over the historical period (1986-2005); this also includes comparisons with observations. Finally in Chapter 4 some climate change results from scenario runs are presented for two of the IPCC standard scenarios; RCP4.5 and RCP8.5.

Throughout the report DMI-HIRHAM5 will be referred to as HIRHAM5, ICHEC-EC-EARTH as EC-EARTH and ECMWF-ERAINT as ERAINT. The data files behind all the maps of model output shown in this report is publically available through ESGF, http://cordexesg.dmi.dk/esgf-web-fe/, in addition to several other parameters not shown in this report.

This report is based on version 2 of the simulation; an error was discovered in the first published simulation, and the entire simulation was redone. Likewise this report was originally published with results based on the first version of the simulation which was found erroneous. This version, v2, is based on the second simulation with the error corrected.

1.1 Acknowledgements

The CORDEX AFR-44 simulation made at the Danish Climate Centre at DMI was funded by the European Union Seventh Framework Programme (FP7/2007-2013) project IMPACT2C.

We acknowledge the use of the GPCP combined precipitation data, which were developed and computed by the NASA/Goddard Space Flight Center's Laboratory for Atmospheres as a contribution to the GEWEX Global Precipitation Climatology Project.

2. Evaluation; ERA-interim run

To evaluate the performance of DMI-HIRHAM5 over the African continent, the RCM have been driven by ECMWF's ERA-interim re-analysis product (Dee *et al.*, 2011; Uppala *et al.*, 2005). This allows for comparison of the RCMs output with observed data as the weather of the RCM should resemble the actual weather of the period. For Africa it should recalled that ground based data are sparse, which affects the quality of both the ERA-interim re-analysis data, and the observational data (see e.g. Figure 2.5). The ERA-interim run spans the period 1989-2010 as prescribed in the CORDEX specifications, which is available on http://cordex.dmi.dk/.

The CORDEX Africa domain, abbreviated AFR-44, has a resolution of 0.44°, and spans from 24.64°W to 60.28°E, and from 45.76°S to 42.24°N, which amounts to 194 gridpoints in the east-west direction, and 201 gridpoints in the north-south direction; more information about the domain can be found in the CORDEX specifications. To account for edge effects the actual simulation was carried out on a grid with at least 10 additional gridpoints in each direction; these have been removed in the maps presented here.

As the observation dataset to which we compare the output of HIRHAM5, we use the UDEL (University of Delaware) dataset (Legates & Willmott, 1990), which is available on http://climate.geog.udel.edu/~climate/. The UDEL dataset is gauge-based and has a spatial resolution of 0.5° and a monthly temporal resolution. We use the latest versions, which at the moment of writing is version 3.01 for temperature (Matsuura & Willmott, 2012a), and version 3.02 for precipitation (Matsuura & Willmott, 2012b). In addition we use the GPCP (Global Precipitation Climatology Project) data set, which is available on http://www.esrl.noaa.gov/psd/data/gridded/data.gpcp.html. It only includes precipitation, but combines observations and satellite precipitation data. It has a spatial resolution of 2.5° and a monthly temporal resolution.

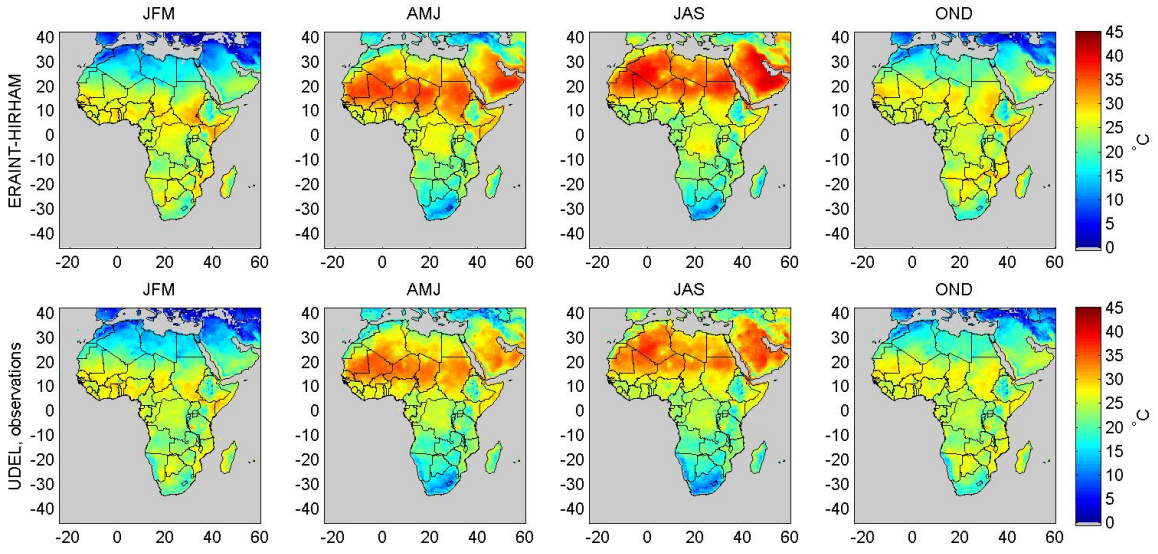

Figure 2.1: Top row shows the seasonal mean 2-m air temperature in °C from 1989-2010 for the ERAINT-HIRHAM5 simulation over Africa. Bottom row shows the seasonal mean temperatures from the UDEL dataset of gridded observations for the same period.

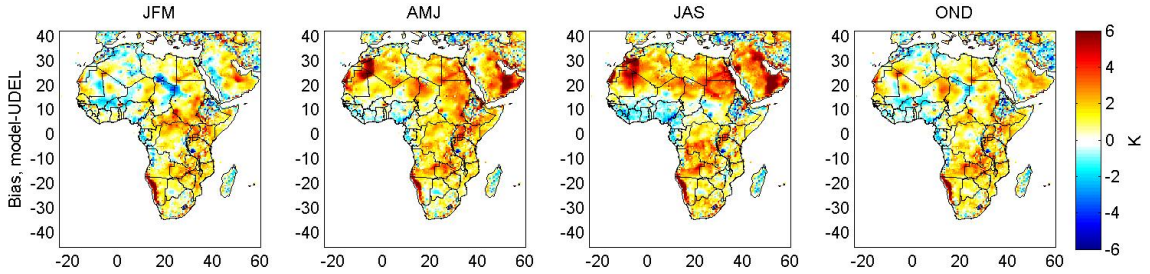

Figure 2.2: The four panels show the seasonal mean bias in 2-m air temperature over Africa for the ERA-interim run covering 1989-2010; bias is calulated as model minus observations. From the figure it is clear that the HIRHAM5 simulation has a warm bias in large parts of Africa varying with season.

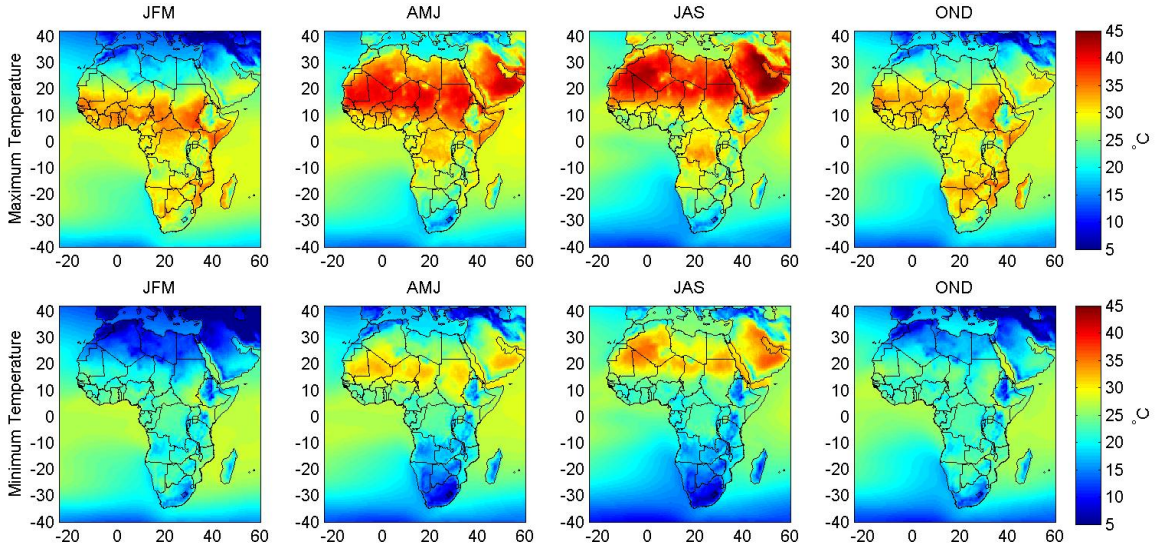

Figure 2.3: The seasonal mean of the daily maximum (top row) and minimum (bottom row) 2-m air temperature in °C for each season for the ERA-interim driven HIRHAM5 simulation from 1989-2010.

The maps shown are all divided into seasons, where we use January-February-March (JFM), April-May-June (AMJ), July-August-September (JAS) and October-November-December (OND). This partition of seasons follow Nikulin *et al.* (2012).

Figure 2.1 shows the seasonal mean 2-m air temperatures for ECMWF-ERAINT - DMI-HIRHAM5 (top row) and the observations from the UDEL dataset (bottom row) for 1989-2010. The temperature bias given as the model output minus the observations is shown in Figure 2.2 for each season. The figure shows that HIRHAM5 has a warm bias of a few degrees in large areas of Africa, particularly in AMJ and JAS. Part of this bias may be due to an erroneous albedo in HIRHAM5 as discussed later in this chapter. In Figure 2.3 the seasonal means of the daily maximum and minimum temperature of the simulation are shown.

Figure 2.4 shows the seasonal mean precipitation for the ERA-interim driven HIRHAM5 simulation and the observations (UDEL dataset) from 1989-2010 for each of the four seasons. The locations of the precipitation observations are shown in Figure 2.5 for January 1990 and January 2000. Note how the number of precipitation stations decrease drastically during the period; an animation showing the number and location of precipitation stations used for the UDEL dataset for each month is available at http://climate.geog.udel.edu/~climate/, where

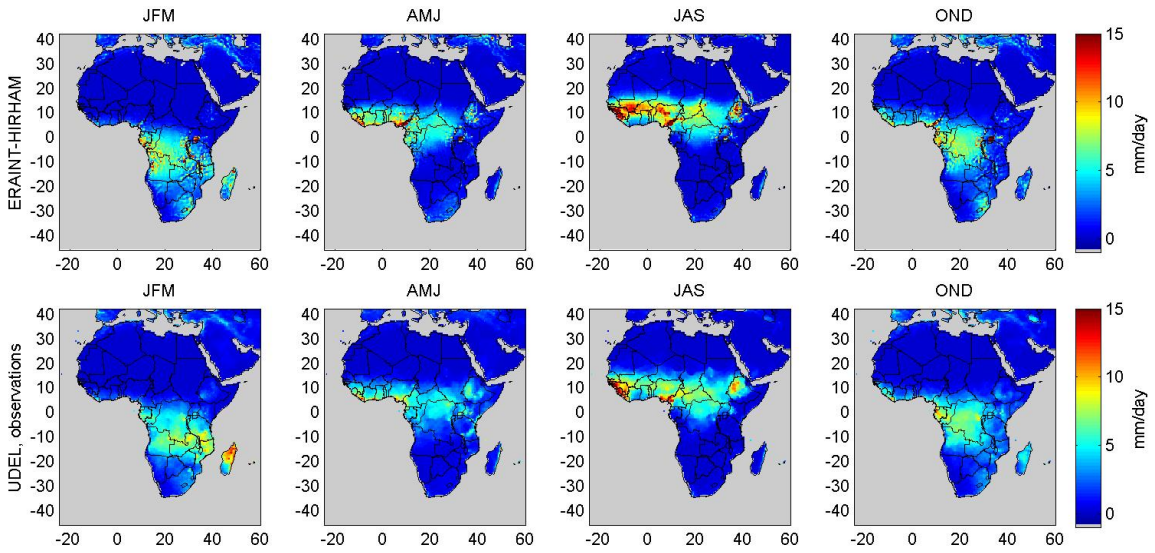

Figure 2.4: The top row of the figure shows the seasonal mean precipitation from ERAINT-HIRHAM5 for 1989-2010 in mm/day. The bottom row shows the seasonal mean precipitation from the UDEL dataset for the same period; the locations of the precipitation stations are shown in Figure 2.5

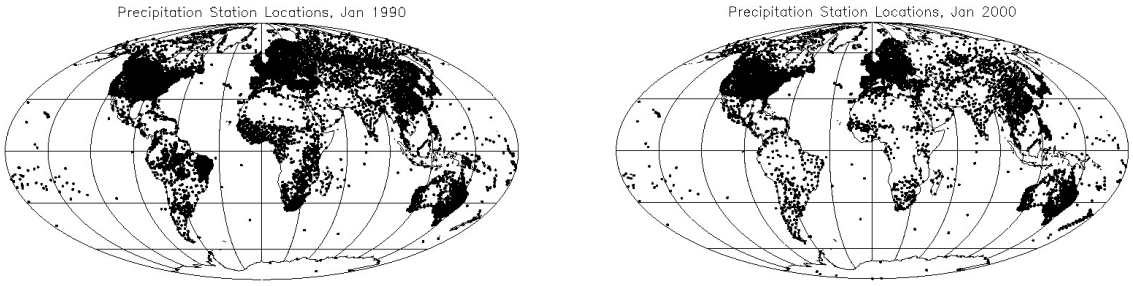

Figure 2.5: The locations of precipitation stations on which the UDEL dataset is based for January 1990 and January 2000. The number of precipitation stations available over Africa is reduced drastically over the period 1985-2010, which includes both the ERA-interim period and the historical run (see Chapter 3). Note also that there are large areas in Africa where no precipitation stations are available, and where the observed values shown in the bottom row of Figure 2.4 are interpolated. These figures are adopted from Matsuura & Willmott (2012b), http://climate.geog.udel.edu/~climate/.

these maps also are taken from. The precipitation bias, i.e. the model results minus the observed values, is shown in Figure 2.6 for both absolute and relative values. The relative bias, calculated as the absolute bias divided by the observed precipitation in each gridpoint, may be very large, particularly where the observed precipitation is very low. HIRHAM5 has a tendency of being too dry (negative bias) in large parts of east Africa with a seasonal variation. In West Africa HIRHAM5 has a wet bias in most seasons. Figure 2.7 shows the monthly mean precipitation for four different countries; Burkina Faso in West Africa, Cameroon around equator, Tanzania in East Africa and Botswana to the south. This Figure shows in more detail how HIRHAM5 captures the seasonality of the precipitation in these four countries, compared to the UDEL and the GPCP gridded observations.

The seasonal mean evaporation in mm/day from ERAINT-HIRHAM5 of 1989-2010 is shown in Figure 2.8. Figure 2.9 shows the seasonal mean of the total runoff (mm/day) and the total

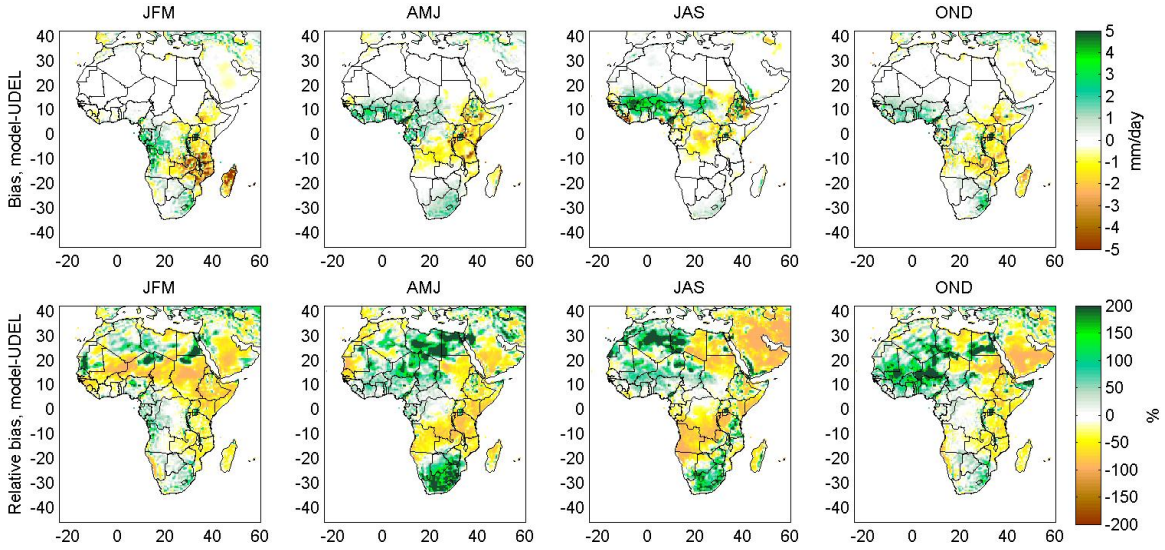

Figure 2.6: The figure shows the precipitation bias of HIRHAM5 (ERAINT-HIRHAM5 minus UDEL observations) in mm/day (top row) and in % (bottom row).The figure shows that HIRHAM5 has a tendency of being too dry in the eastern part of Africa most of the year and too wet in West Africa.

soil moisture content (kg/m^2). Figure 2.10 shows the seasonal mean specific humidity, the relative humidity in %, the surface wind speed in m/s (at 10-m), the total cloud cover in % and the downwelling shortwave radiation at the surface in W/m^2. In Figure 2.11 seasonal means of $q \cdot \vec{v}$ at 850hPa are shown; these plots indicate the transport of moisture across the continent.

Figure 2.12 shows the seasonal mean albedo of the DMI-HIRHAM5 simulation (top row) and of observed black-sky albedo (middle row) from CFSAM data from Deutscher Wetterdienst (DWD). The seasonal variation in the albedo in HIRHAM5 is very small, and there is practically no interannual variability; only snow cover changes albedo in HIRHAM5, and the snow cover in Africa is limited to few mountain tops. The bottow row of Figure 2.12 shows the bias, i.e. HIRHAM5's albedo minus the observed, and in general we see that the albedo of the model is lower than the observed, particularly in Northern Africa by about 0.1 to 0.2 or more. A too low albedo results in a too strong warming of the surface in the model, and this could at least be part of the reason of the warm bias over northern Africa shown in Figure 2.2.

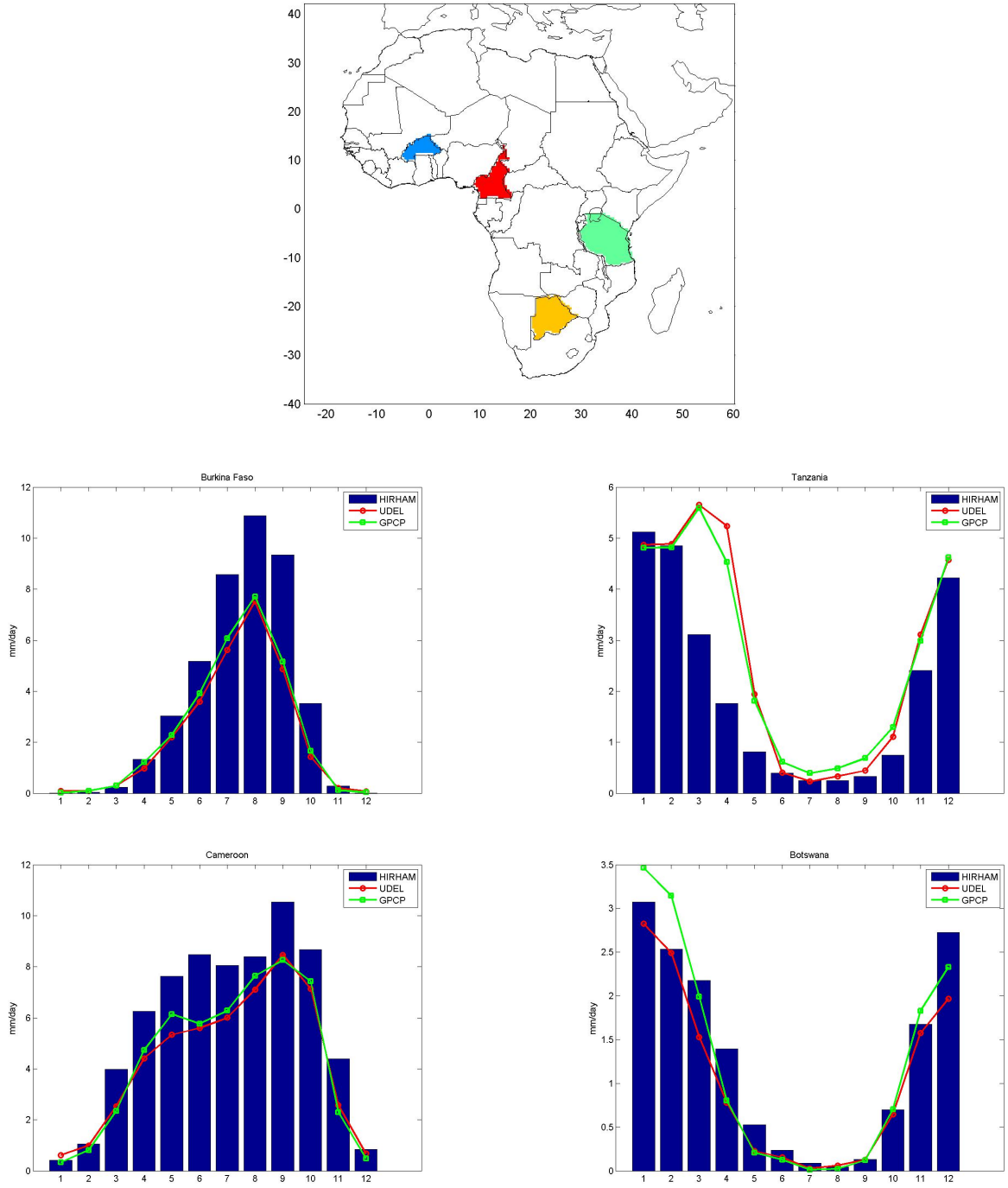

Figure 2.7: The monthly mean precipitation (in mm/day) from January (M1) to December (M12) from four different countries from 1989-2010 for the ERAINT-HIRHAM simulation and from the UDEL and the GPCP data sets. The map in the top shows the locations of Burkina Faso (blue), Cameroon (red), Tanzania (green) and Botswana (orange).

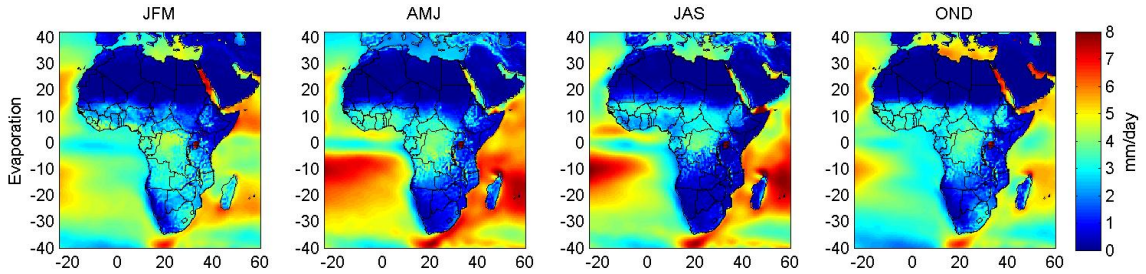

Figure 2.8: The figure shows the simulated seasonal mean evaporation in mm/day over the period 1989-2010.

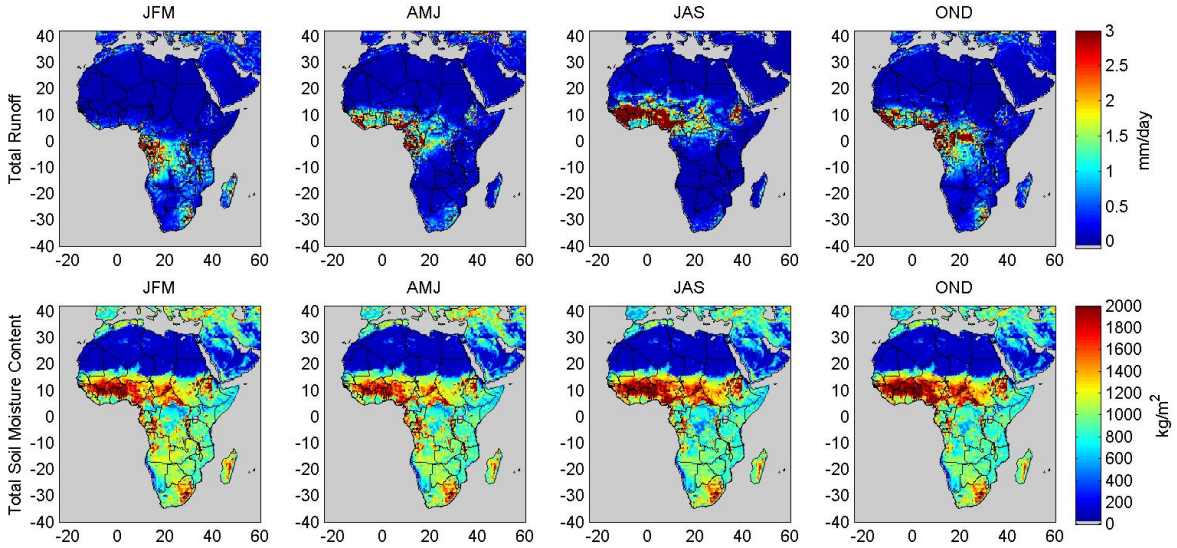

Figure 2.9: The simulated seasonal mean total runoff in mm/day (top row) and total soil moisture content in kg/m^2 (bottom row) from ERAINT-HIRHAM5 over the period 1989-2010.

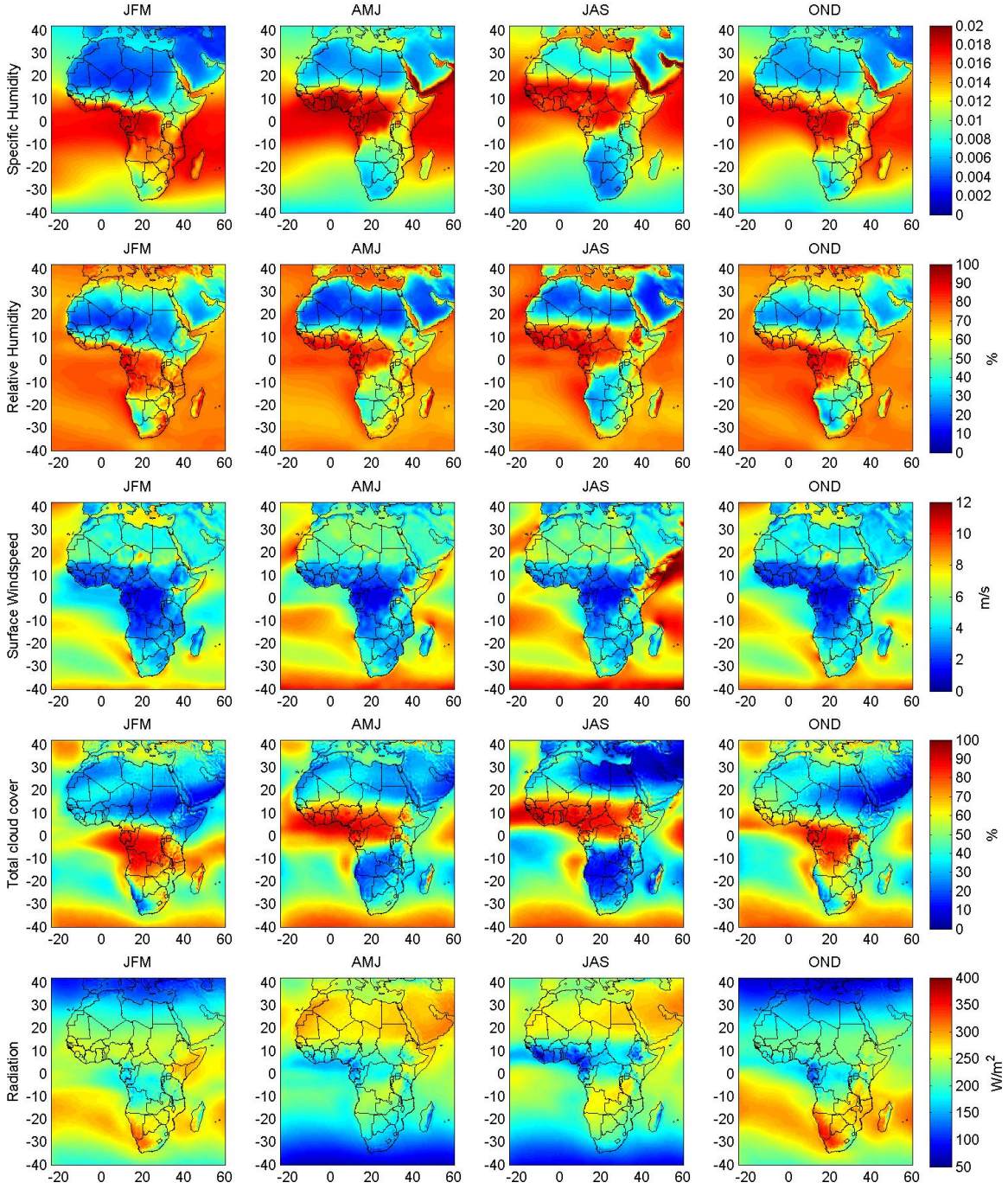

Figure 2.10: Top row: The seasonal mean specific humidity of the ERA-interim driven HIRHAM5 simulation over the period 1989-2010. Second row: The relative humidity in %. Third row: The seasonal mean 10-m surface wind speed in m/s. Fourth row: The total cloud cover in %. Bottom row: The simulated seasonal mean of the surface downwelling shortwave radiation in W/m^2.

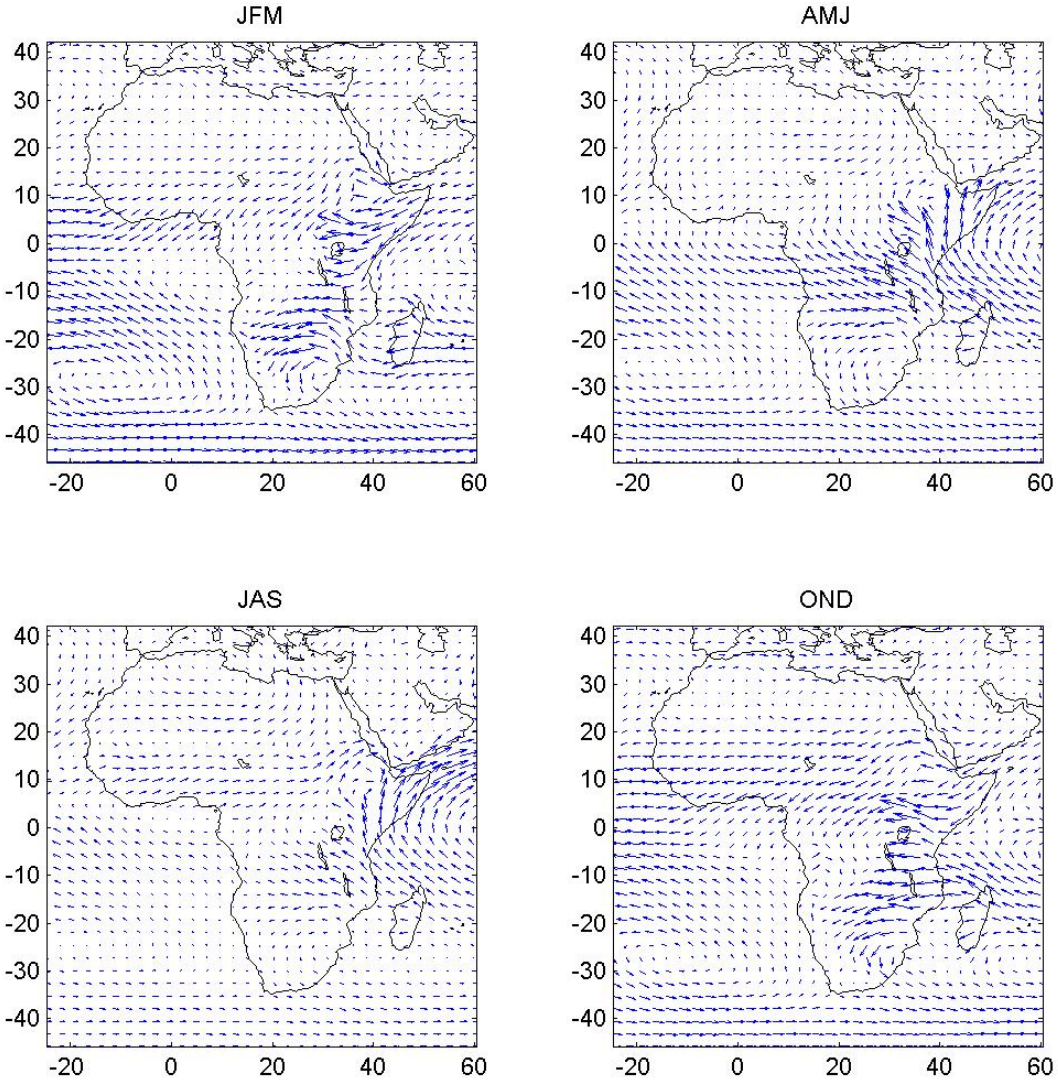

Figure 2.11: The figure shows seasonal means of q· $\vec{v}$ at 850hPa from ERAINT-HIRHAM5 for 1989-2010.

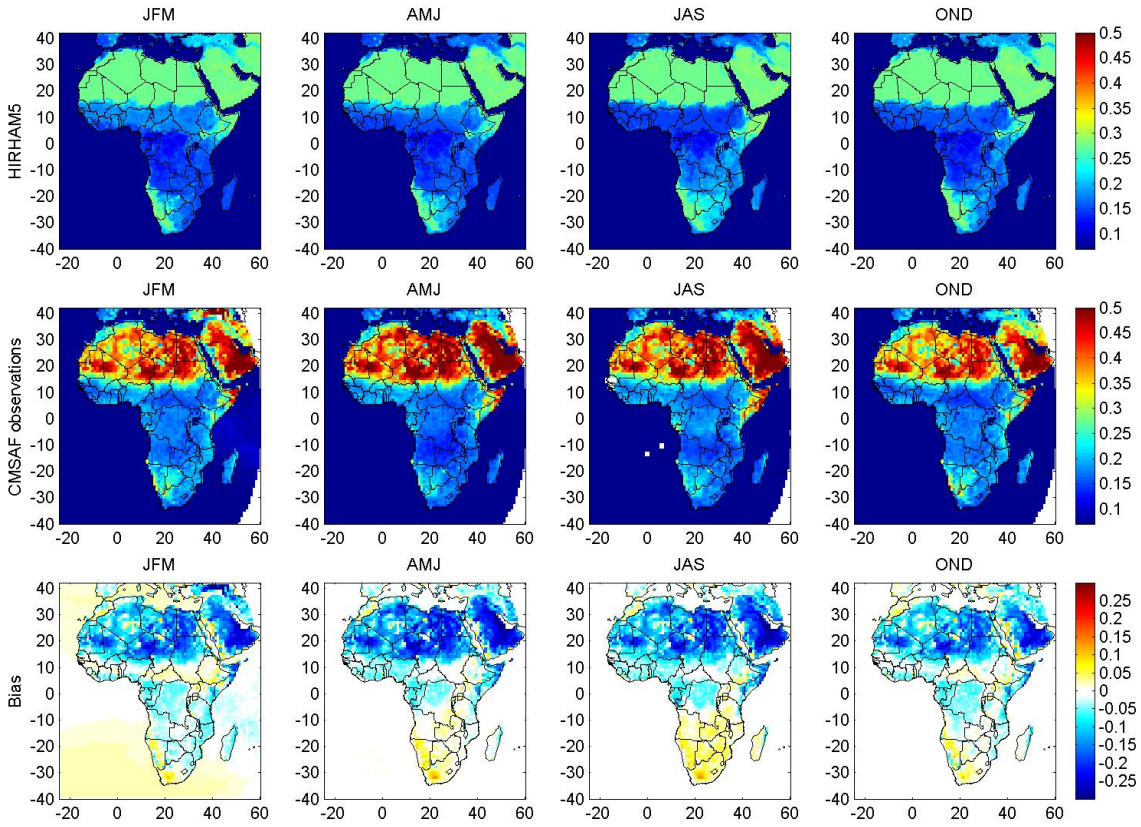

Figure 2.12: The top row shows the seasonal mean albedo used by HIRHAM5, the middle row shows the observed seasonal mean albedo from CFSAM, and the bottom row is the bias, e.g. the HIRHAM5's albedo minus the observed; all plots in this figure cover the years 2008-2010.

3. Historical run

Following the CORDEX specifications, a historical simulation covering the period 1951-2005 has been carried out. For this simulation HIRHAM5 has been driven by a historical run of EC-EARTH where observed green house gas inventory and aerosol loading have been fed into the global model in the extent observations were available. Here we will show some results for the historical time-slice 1986-2005; this time-slice is chosen to comply with the focus time-slices of the 5th IPCC report. The historical time-slice overlaps considerably with the evaluation time-slice, 1989-2010, the main difference here is that the historical time-slice is GCM-driven whereas the evaluation time-slice is driven by re-analysis data.

Figure 3.1 shows the seasonal mean 2-m air temperature, the mean of daily maximum and the mean of the daily minimum temperature of the GCM-RCM simulation, all in °C, from 1986-2005. As expected the seasonal means of the baseline period is very similar to the seasonal mean of the evaluation period, shown in Figure 2.1 and 2.3. Figure 3.2 shows the bias, i.e. model minus observations, compared to the UDEL dataset. The figure shows that the EC-EARTH driven HIRHAM5 simulation generally is too cold, particularly in JFM and OND, but also in AMJ. The fact that the bias of the historical simulation generally is negative whereas the bias of the ERAINT simulation generally is positive (see Figure 2.2) indicates that the cold bias primarily is introduced by EC-EARTH.

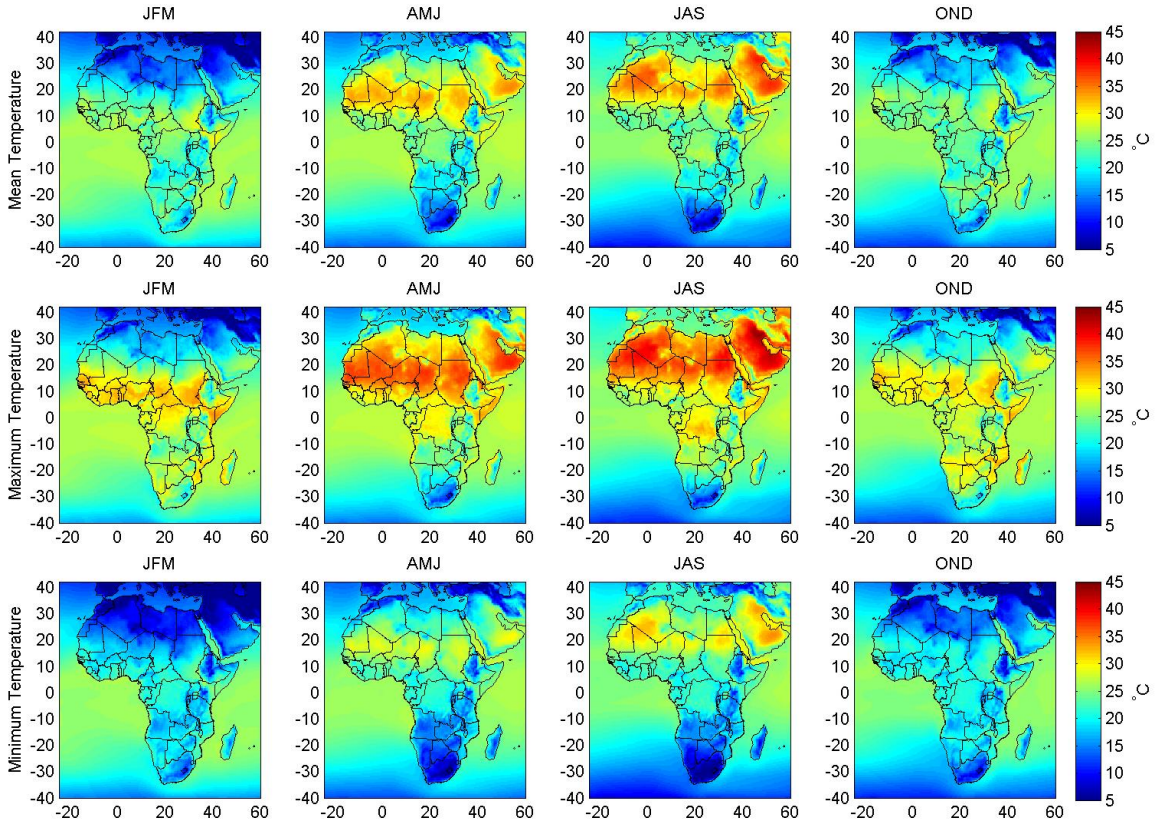

Figure 3.1: The top row shows the simulated seasonal mean 2-m air temperature in °C, the middle and bottom row show the mean of daily maximum and minimum temperature, respectively. Everything is based on EC-EARTH-HIRHAM5 for the baseline period, 1986-2005.

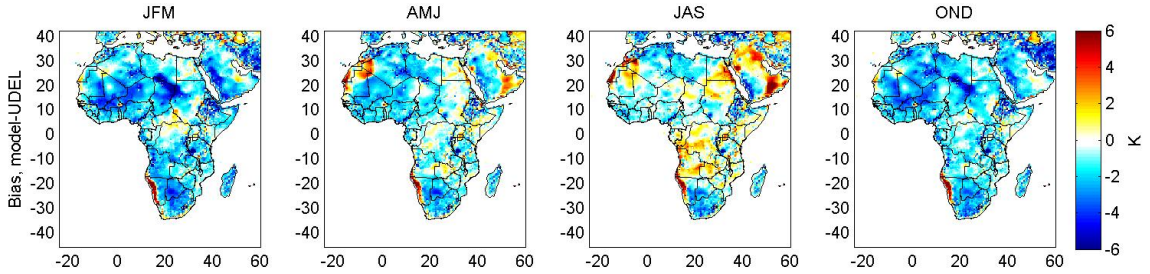

Figure 3.2: The difference between the simulated seasonal mean 2-m air temperature (top row of Figure 3.1) and observed 2-m air temperature from the UDEL dataset (bottom row of Figure 2.1) from 1986-2005.

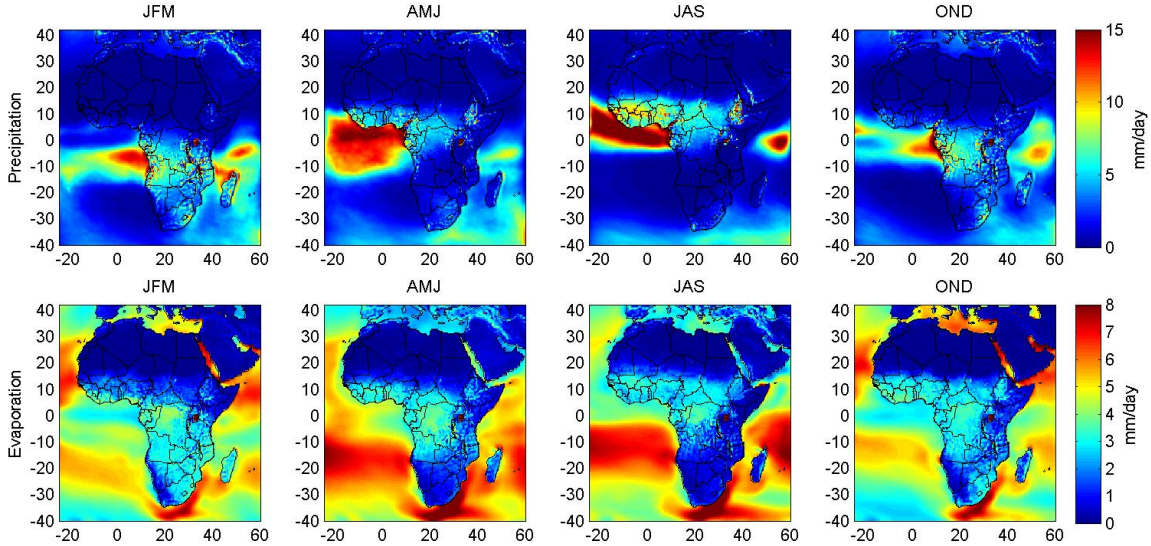

Figure 3.3: The simulated seasonal mean precipitation (top row) and evaporation (bottom row) in mm/day from EC-EARTH-HIRHAM5 for the historical baseline period, 1986-2005.

Figure 3.3 shows the seasonal mean precipitation and evaporation in mm/day for 1986-2005, and Figure 3.4 shows the monthly variation of precipitation from four different countries across Africa compared to both the UDEL and the GPCP data sets. Figure 3.5 shows the precipitation bias of the EC-EARTH driven HIRHAM5 simulation compared to the UDEL dataset based on observations (model minus observations). The seasonal variation and the geographical pattern of the bias on the historical run resembles the bias on the ERA-interim driven HIRHAM5 simulation shown in Figure 2.6; the GCM driven HIRHAM5 simulation does, however, have a stronger wet bias in South Africa.

Figure 3.6 shows the seasonal mean of the total runoff (mm/day) and the total soil moisture content (kg/m^2) for EC-EARTH-HIRHAM5 from 1986-2005. Figure 3.7 shows seasonal mean specific humidity, relative humidity (%), surface wind speed at 10 m (m/s) and shortwave downwelling radiation at the surface (W/m^2) for the baseline period 1986-2005. Figure 3.8 shows the seasonal means of the specific humidity multiplied by the wind velocity at 850hPa for the historical run from 1986-2005. This indicates the transport of humidity across the continent in the simulation.

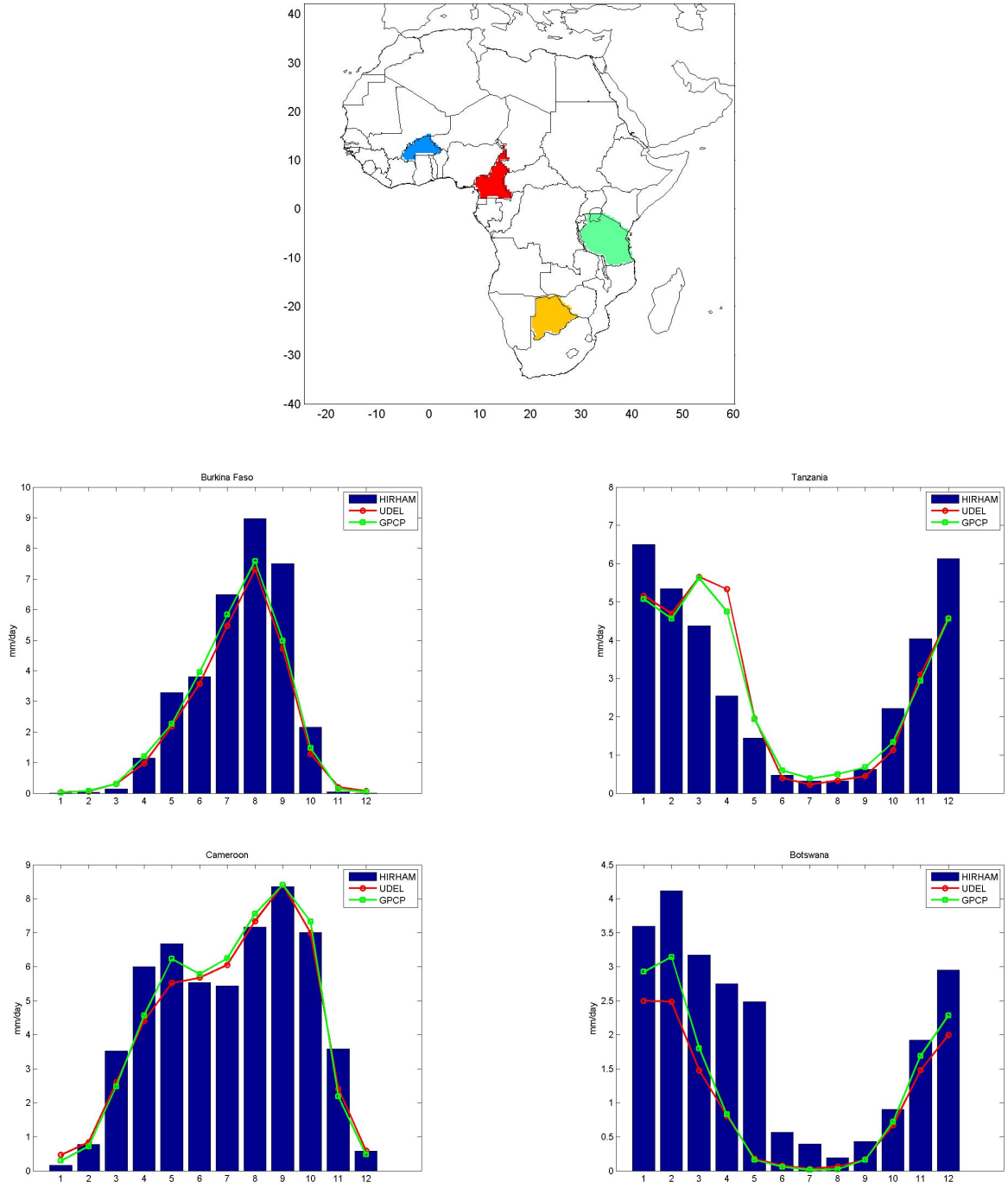

Figure 3.4: The monthly mean precipitation (in mm/day) from January (M1) to December (M12) from four different countries from 1986-2005 for the ECEARTH-HIRHAM simulation and from the UDEL and the GPCP data sets. The map in the top shows the locations of Burkina Faso (blue), Cameroon (red), Tanzania (green) and Botswana (orange).

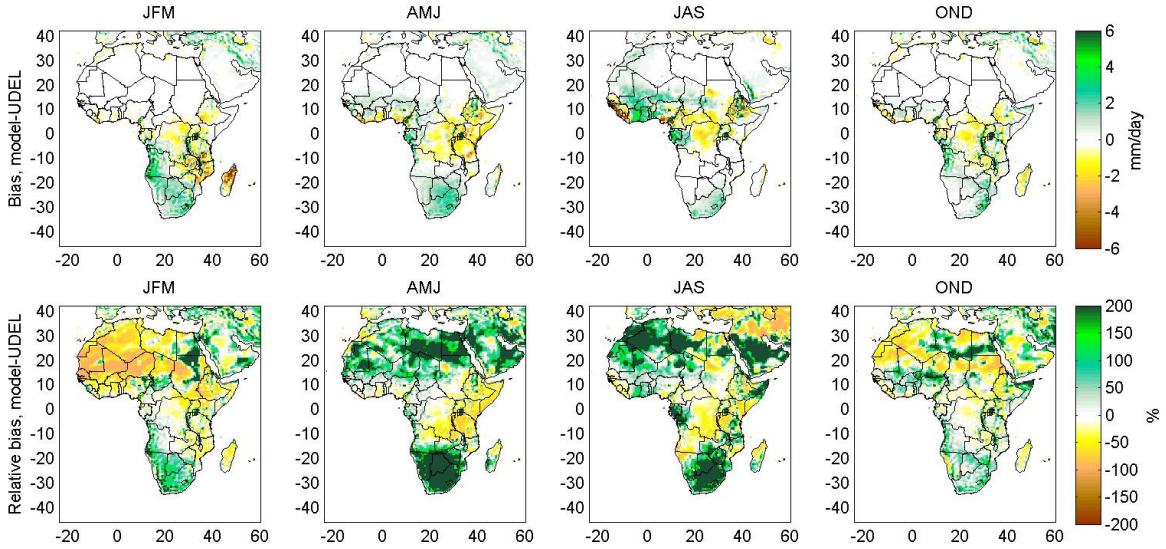

Figure 3.5: The top row shows difference between the simulated seasonal mean precipitation from EC-EARTH-HIRHAM5 (Figure 3.3) and the UDEL dataset (shown in Figure 2.4) in mm/day for the historical baseline period, 1986-2005. The bottom row shows the relative difference in %; note that in some areas where the observed precipitation is very low, the relative difference may be very high, although the absolute difference is small. The locations of the precipitation stations used for the UDEL dataset are shown in Figure 2.5.

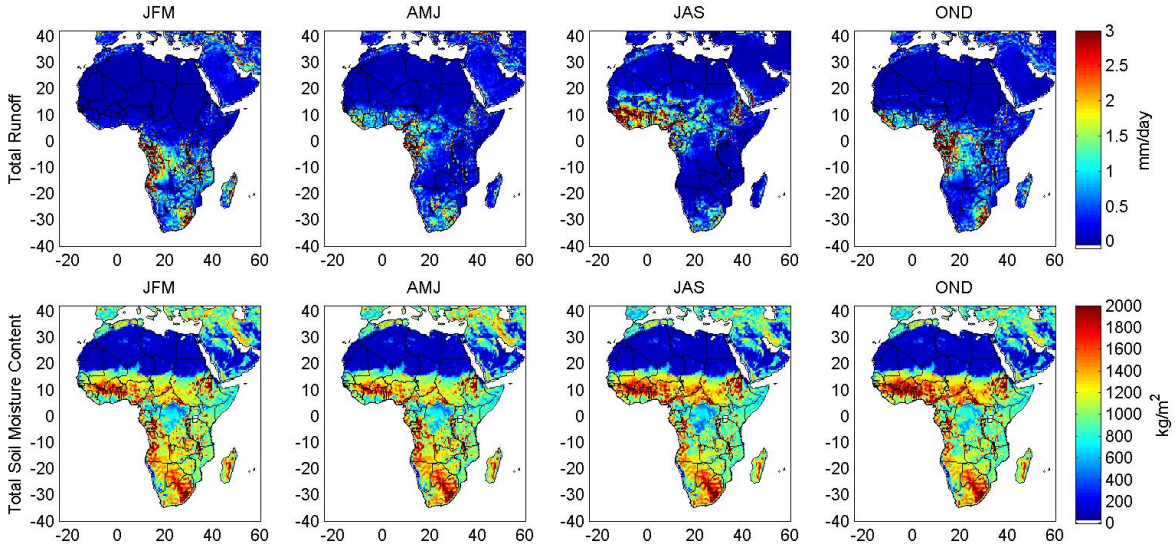

Figure 3.6: The simulated seasonal mean total runoff in mm/day (top row) and total soil moisture content in kg/m^2 (bottom row) from EC-EARTH-HIRHAM5 for the historical baseline period, 1986-2005.

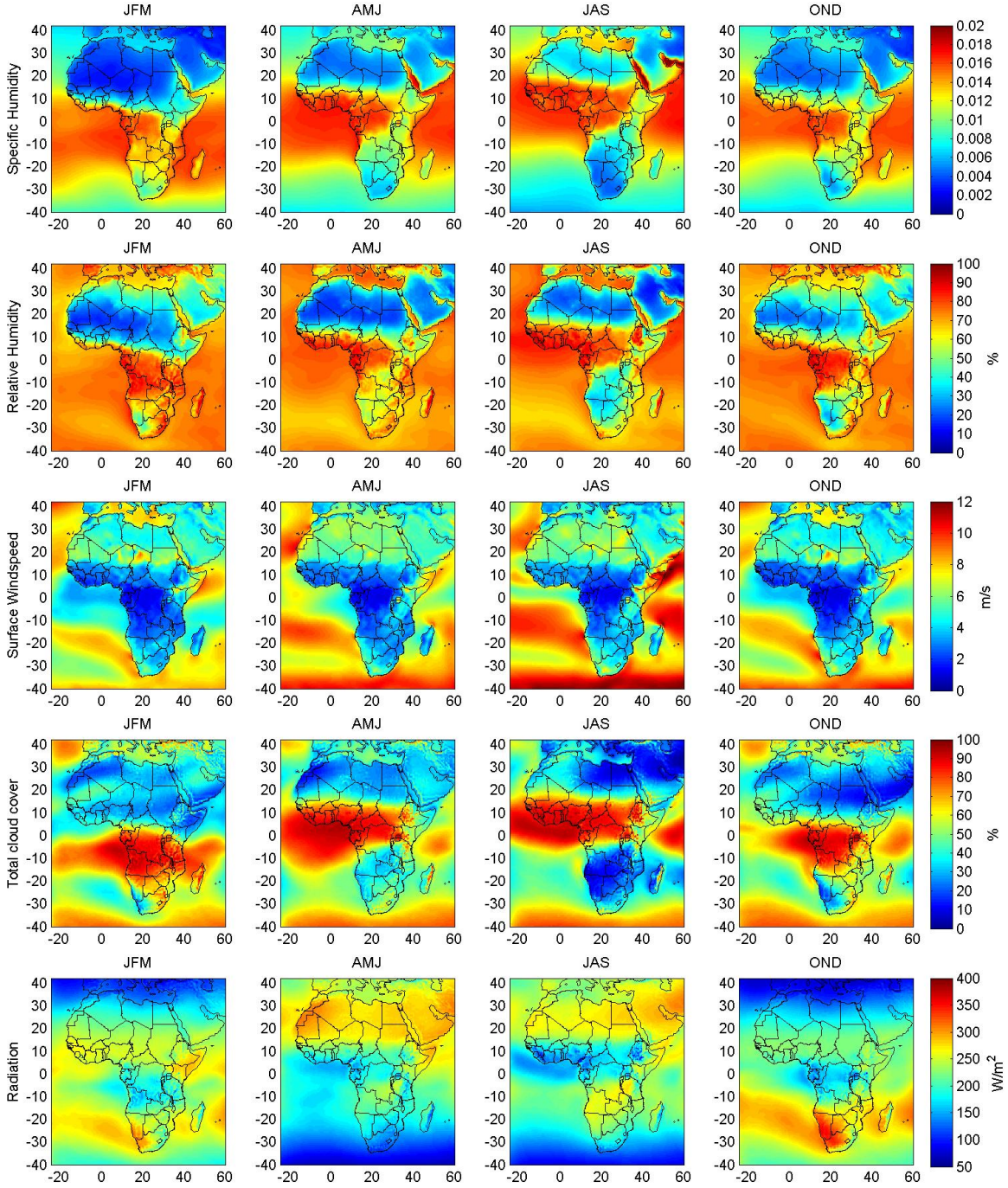

Figure 3.7: Seasonal means from EC-EARTH-HIRHAM5 for the baseline period, 1986-2005. Top row: Specific humidity. Second row: Relative humidity in %. Third row: Surface (10-m) wind speed in m/s. Fourth row: Total cloud cover in %. Bottom row: Downwelling shortwave radiation at the surface in (W/m^2).

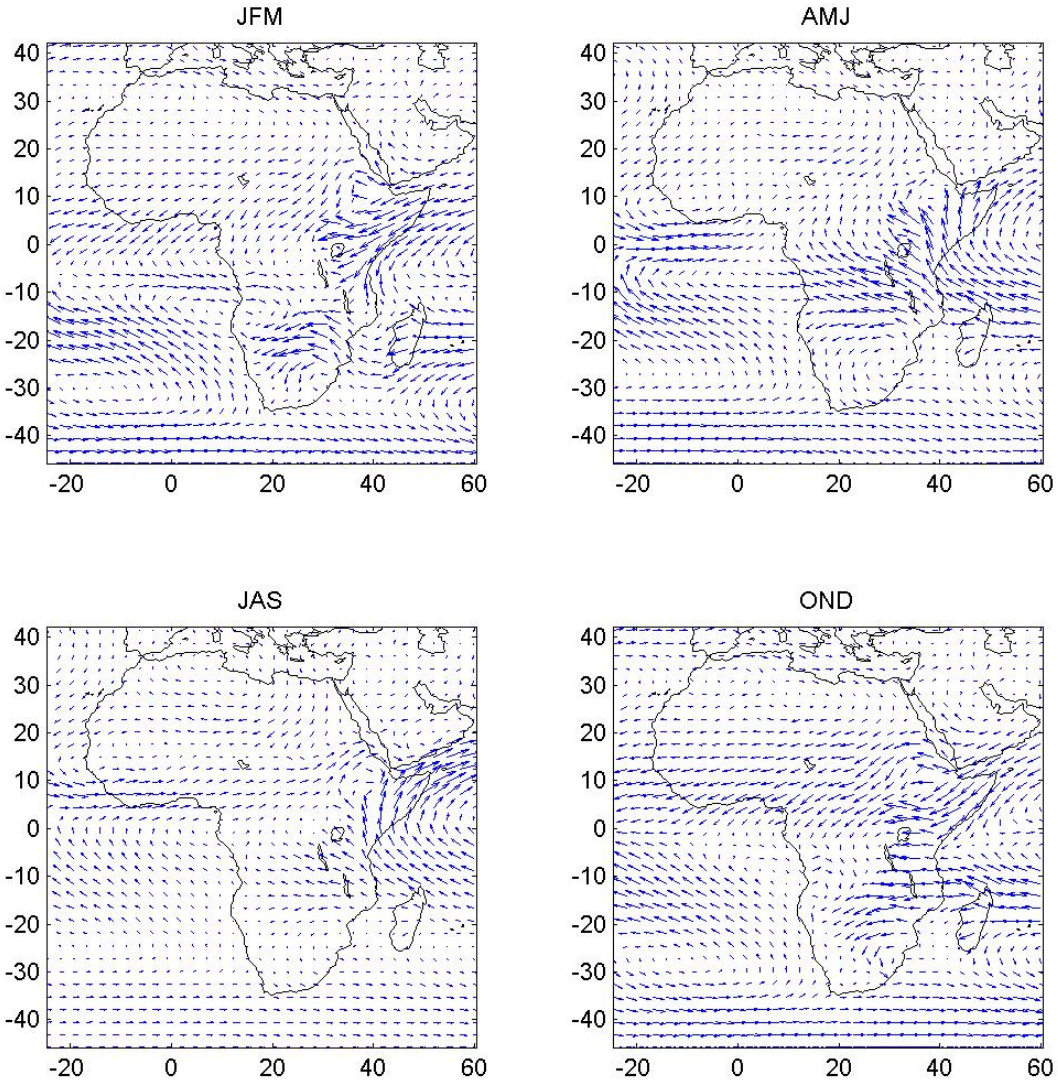

Figure 3.8: The figure shows seasonal means of q· $\vec{v}$ at 850hPa from EC-EARTH-HIRHAM5 for the baseline period, 1986-2005.

4. Future scenario simulations

To look at the projected climate change we have used two different scenarios; RCP4.5 and RCP8.5. EC-EARTH - HIRHAM5 has been run for each of these two scenarios from 2006 to 2100 continued seemlessly from the historical run. In this report we will focus on the projected climate changes in three different future time-slices 2016-2035, 2046-2065 and 2081-2100, following the 5th IPCC report.

Figure 4.1 shows the projected changes in the seasonal mean temperature in K for three different future time-slice (2016-2035, 2046-2065 and 2081-2100) compared to the baseline time-slice 1986-2005. The same thing but for RCP8.5 is shown in Figure 4.2. The projected change of the mean of the daily maximum temperature is shown in Figure 4.3 for RCP4.5 and in Figure 4.4 for RCP8.5, and the projected changes of daily minimum temperature is shown in Figure 4.5 for RCP4.5 and in Figure 4.6 for RCP8.5. These figures show that projected changes in the seasonal means of the daily maximum and daily minimum temperature are very similar to the projected change in the seasonal mean mean temperatur, and that the temperature change at the end of the century is much higher in the RCP8.5 scenario than in the RCP4.5 scenario.

The projected changes in the seasonal mean precipitation is shown in Figure 4.7 for RCP4.5 and Figure 4.8 for RCP8.5. Both absolute and relative changes are shown. Where the

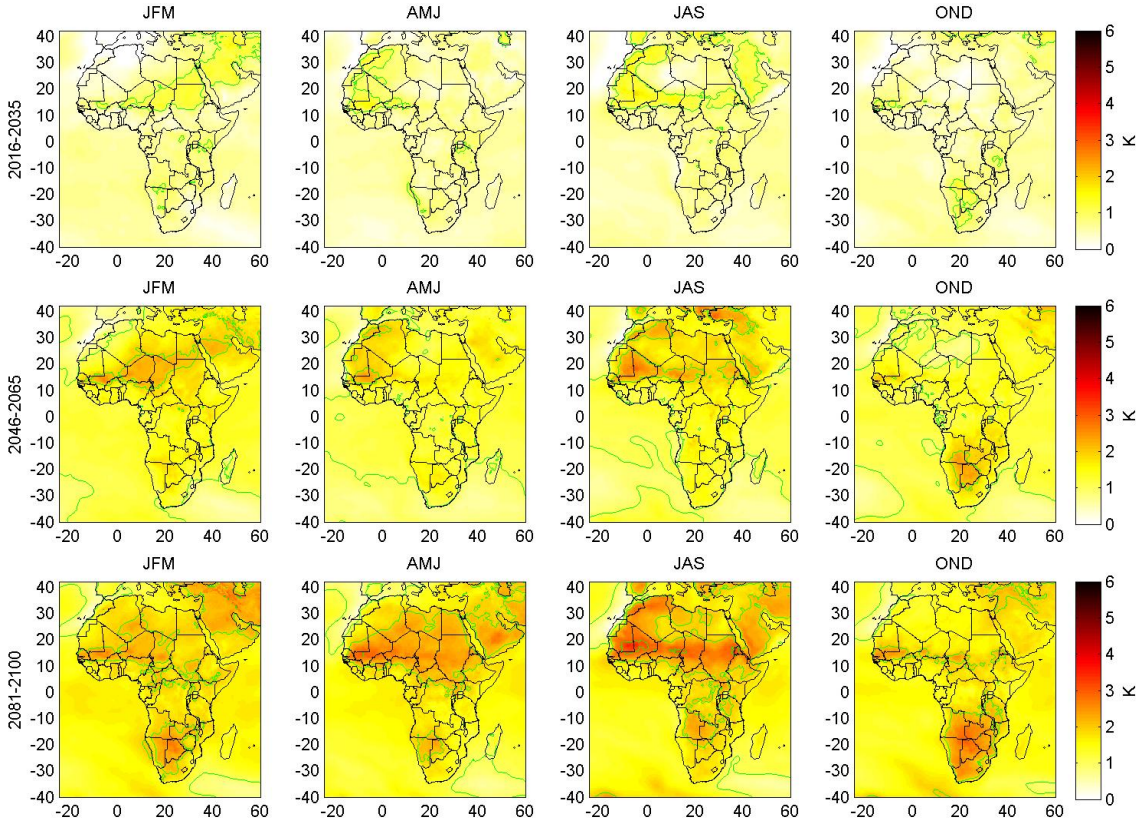

Figure 4.1: Projected temperature change (in K) according to RCP4.5 scenario for three different future time-slices (2016-2035, 2046-2065 and 2081-2100) compared to the baseline time-slice 1986-2005. The green contours mark 1, 2, 3, 4 and 5 K.

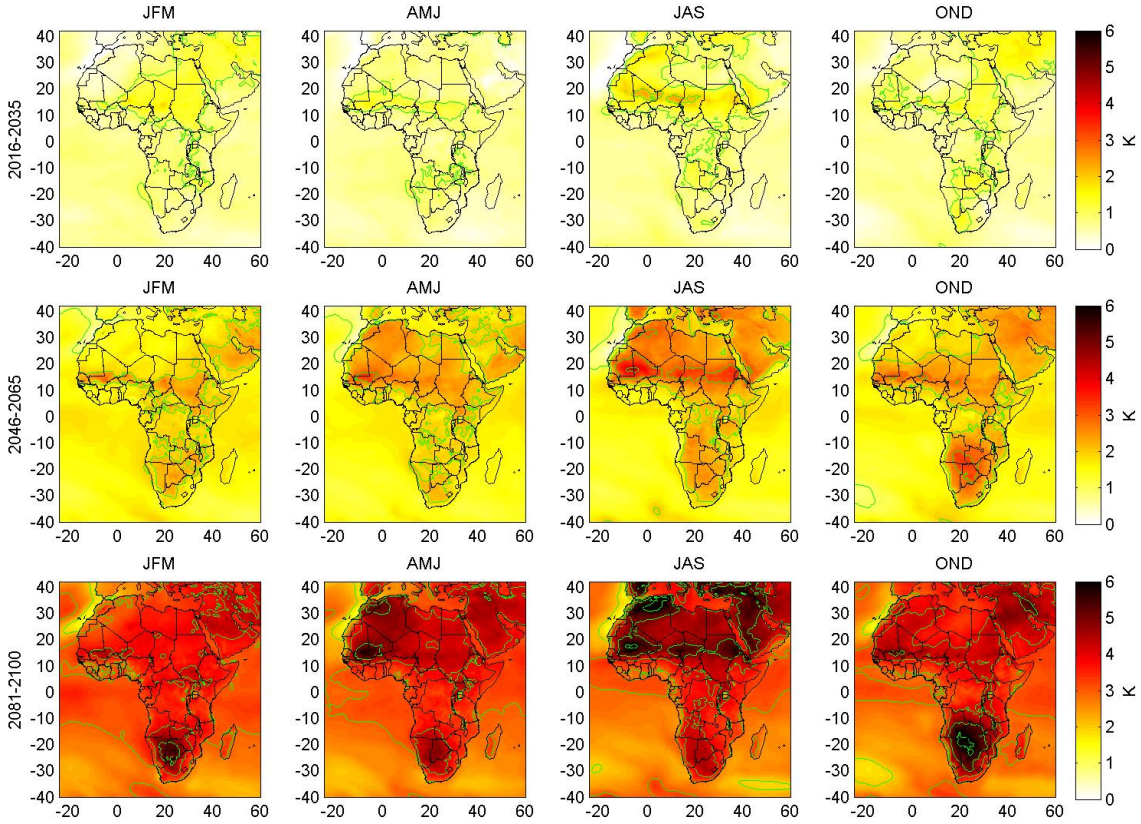

Figure 4.2: Projected temperature change (in K) according to RCP8.5 for three different future time-slices (2016-2035, 2046-2065 and 2081-2100) compared to the baseline time-slice 1986-2005. The green contours mark 1, 2, 3, 4 and 5 K.

seasonal mean precipitation in the historical time-slice is very low, the relative precipitation change can be very large for even very small absolute changes. To avoid spurios features in the maps arising from this, the relative change is only calculated in grid-points, where the seasonal mean precipitation of the historical time-slice is above 0.05 mm/day. Areas where the precipitation of the historical time-slice was less than 0.05 mm/day, are crossed with red in the maps, and the relative changes are not shown.

Figure 4.9 and 4.10 shows the projected absolute and relative changes in evaporation for RCP4.5 and RCP8.5, respectively. Again three future time-slices, 2016-2035, 2046-2065 and 2081-2100, are considered. As the evaporation in some regions is very small, and in particular, was very small in the historical time-slice (Figure 3.3), some of the relative changes appear/are very large.

Figure 4.11 and 4.12 shows the projected absolute and relative changes in total runoff. Note that the very small absolute values of runoff in the historical time-slice (Figure 3.6) cause very large relative changes. Figure 4.13 and 4.14 shows the projected absolute and relative changes in total soil moisture content in kg/m^2 for RCP4.5 and RCP8.5, respectively. A clear trend is evident in the simulated total soil moisture content which decreases in most parts of Africa through the century; the trend is stronger for RCP8.5 than for RCP4.5.

Figure 4.15 and 4.16 shows the projected absolute and relative changes in specific humidity for RCP4.5 and RCP8.5, respectively. In the early time-slice some negative trends are seen in both scenarios but with very small absolute values; it is possibly due to decadal variability.

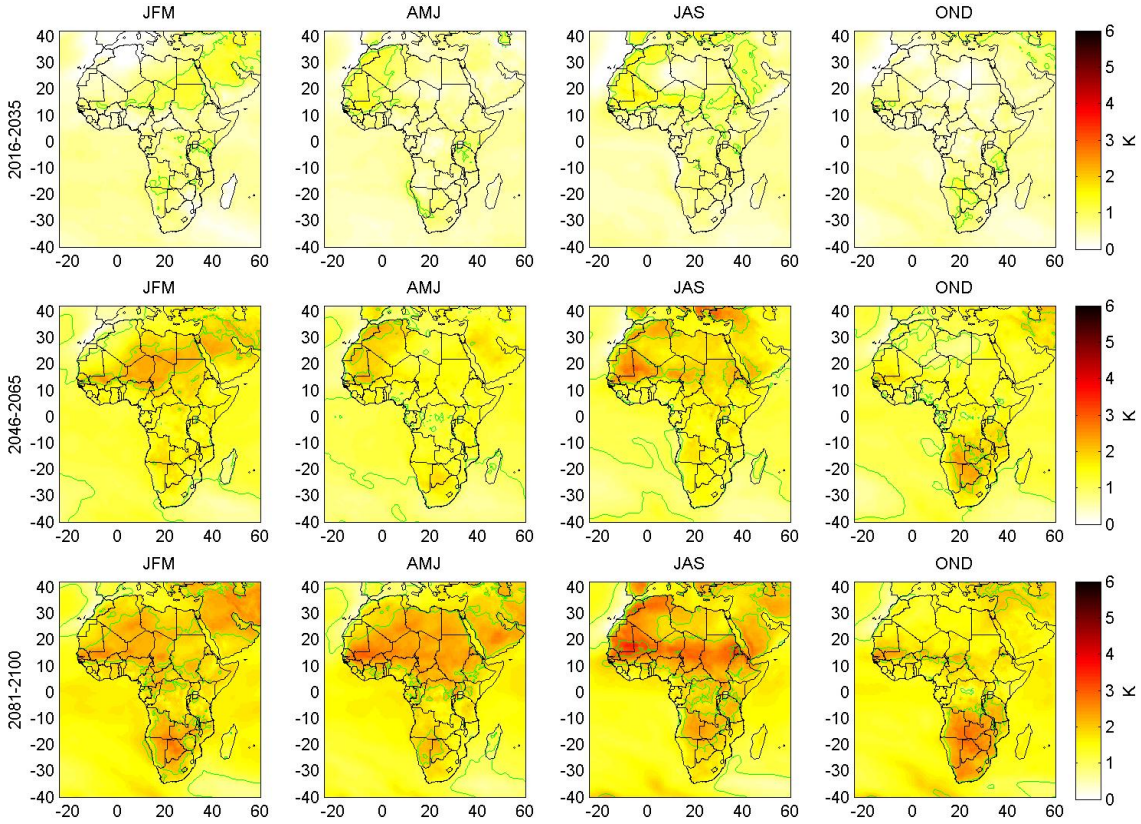

Figure 4.3: Projected change of the seasonal mean of the daily maximum temperature (in K) according to RCP4.5 for three different future time-slices (2016-2035, 2046-2065 and 2081-2100) compared to the baseline time-slice 1986-2005. The green contours mark 1, 2, 3, 4 and 5 K.

The trend in specific humidity is very clear; it is increasing with time, more for RCP8.5 than for RCP4.5.

Figure 4.17 and 4.18 shows the projected absolute and relative changes in surface windspeed (at 10 m) for RCP4.5 and RCP8.5, respectively. The trend in windspeed is varying across the continent, but a strong coherent feature is an increase in windspeed in West Africa in JAS.

Figure 4.19 and 4.20 shows the projected absolute and relative changes in shortwave downwelling radiation at the surface in W/m^2 for RCP4.5 and RCP8.5, respectively. The strongest feature here is an increase in the shortwave downwelling radiation at the surface between 10°S and 10°N in JAS towards the end of the century, particularly in RCP8.5.

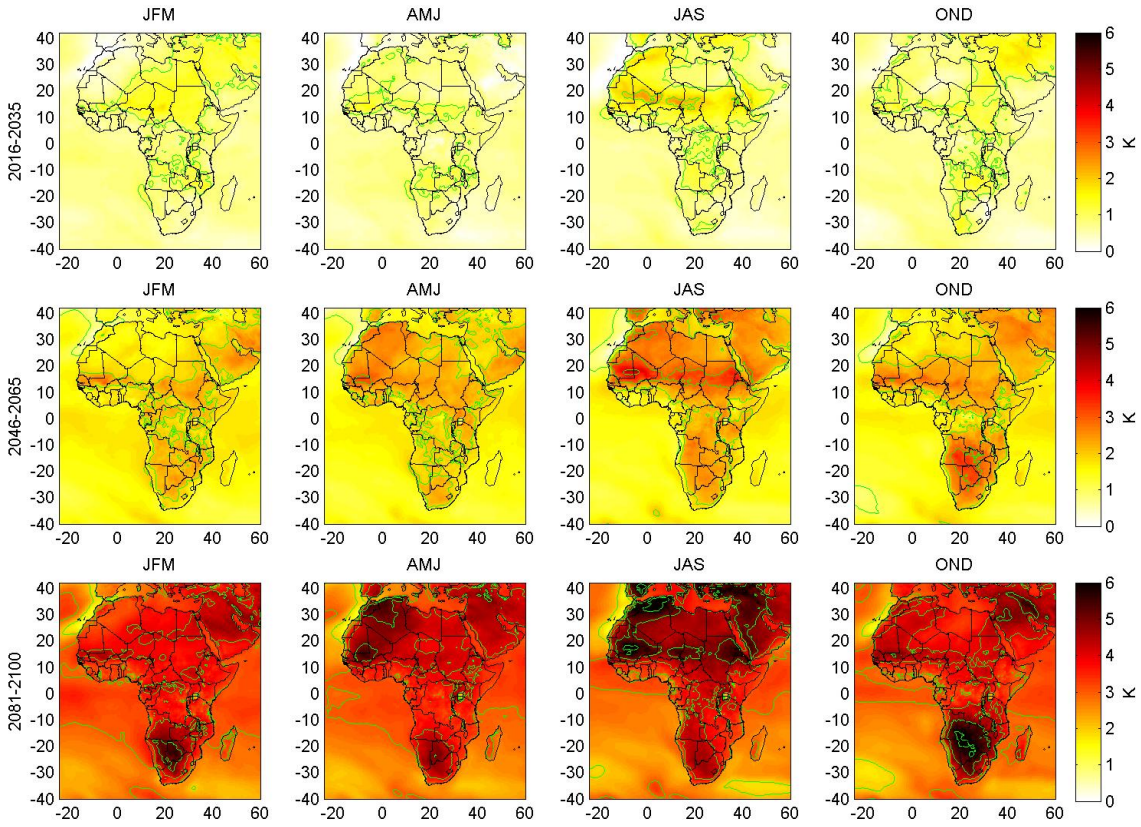

Figure 4.4: Projected change of the seasonal mean of the daily maximum temperature (in K) according to RCP8.5 for three different future time-slices (2016-2035, 2046-2065 and 2081-2100) compared to the baseline time-slice 1986-2005. The green contours mark 1, 2, 3, 4 and 5 K.

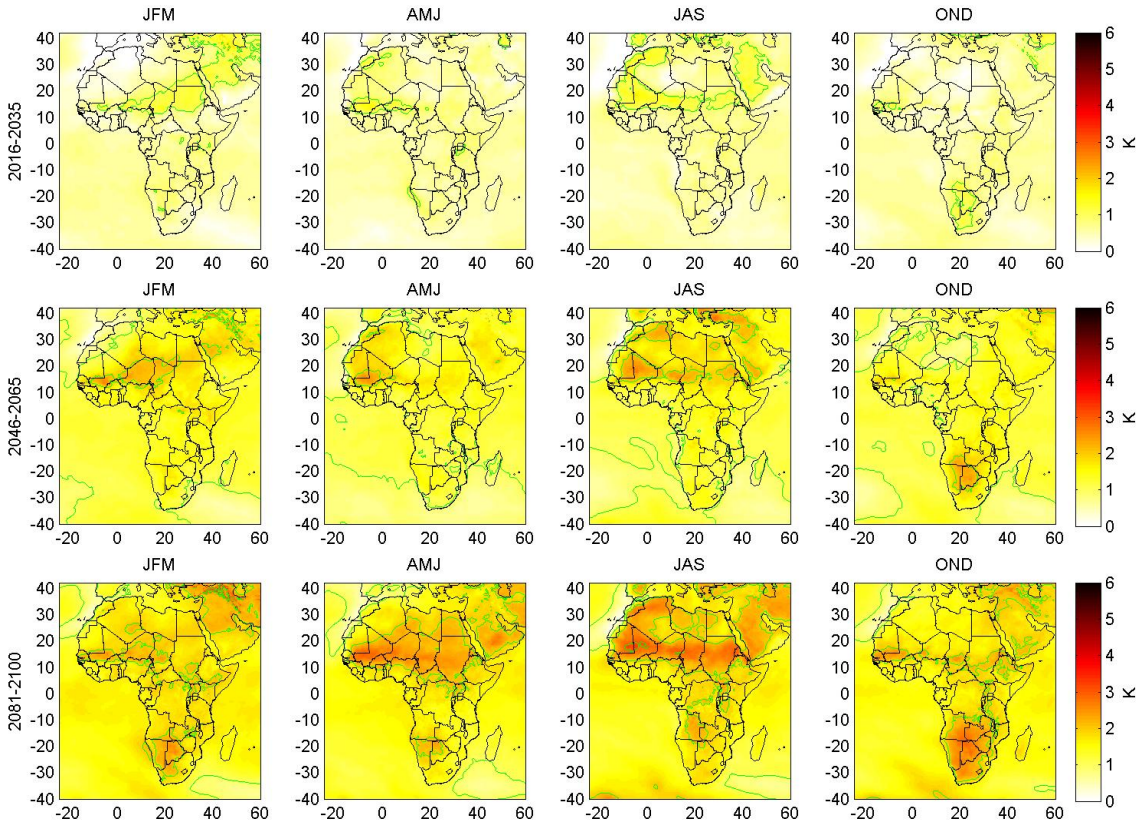

Figure 4.5: Projected change of the seasonal mean of the daily minimum temperature (in K) according to RCP4.5 for three different future time-slices (2016-2035, 2046-2065 and 2081-2100) compared to the baseline time-slice 1986-2005. The green contours mark 1, 2, 3, 4 and 5 K.

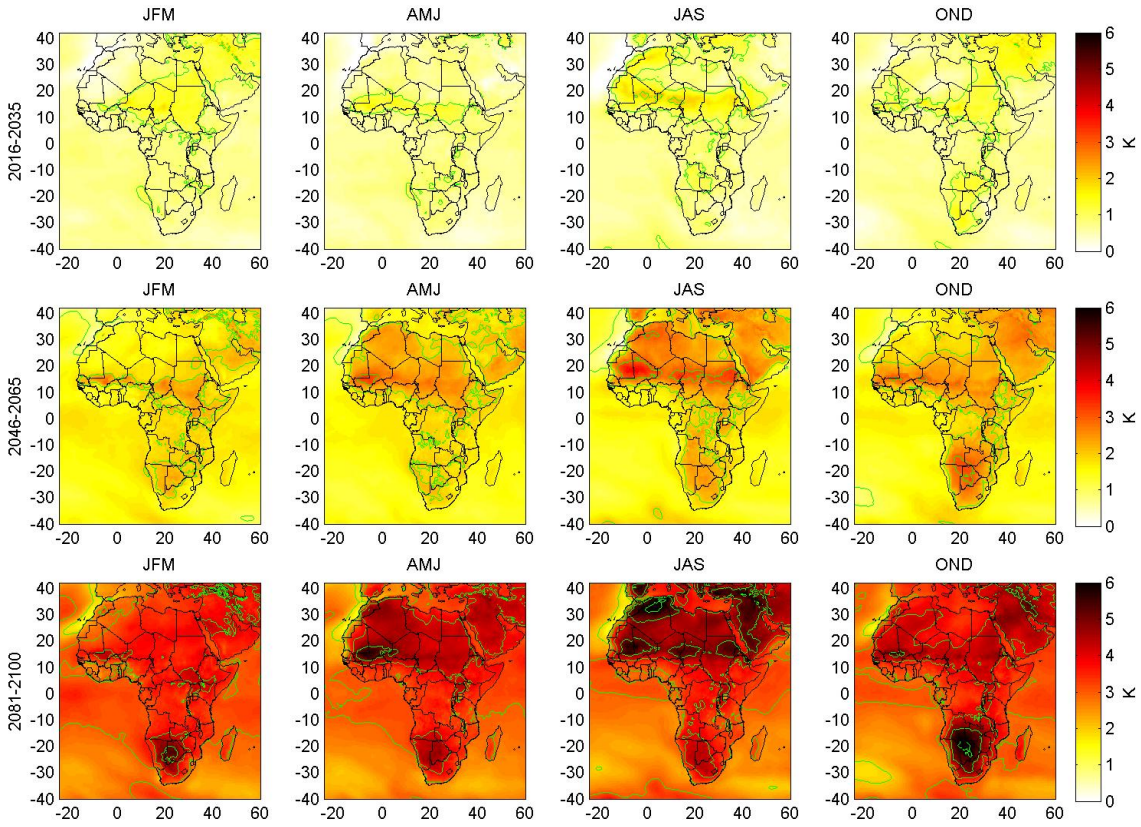

Figure 4.6: Projected change of the seasonal mean of the daily minimum temperature (in K) according to RCP8.5 for three different future time-slices (2016-2035, 2046-2065 and 2081-2100) compared to the baseline time-slice 1986-2005. The green contours mark 1, 2, 3, 4 and 5 K.

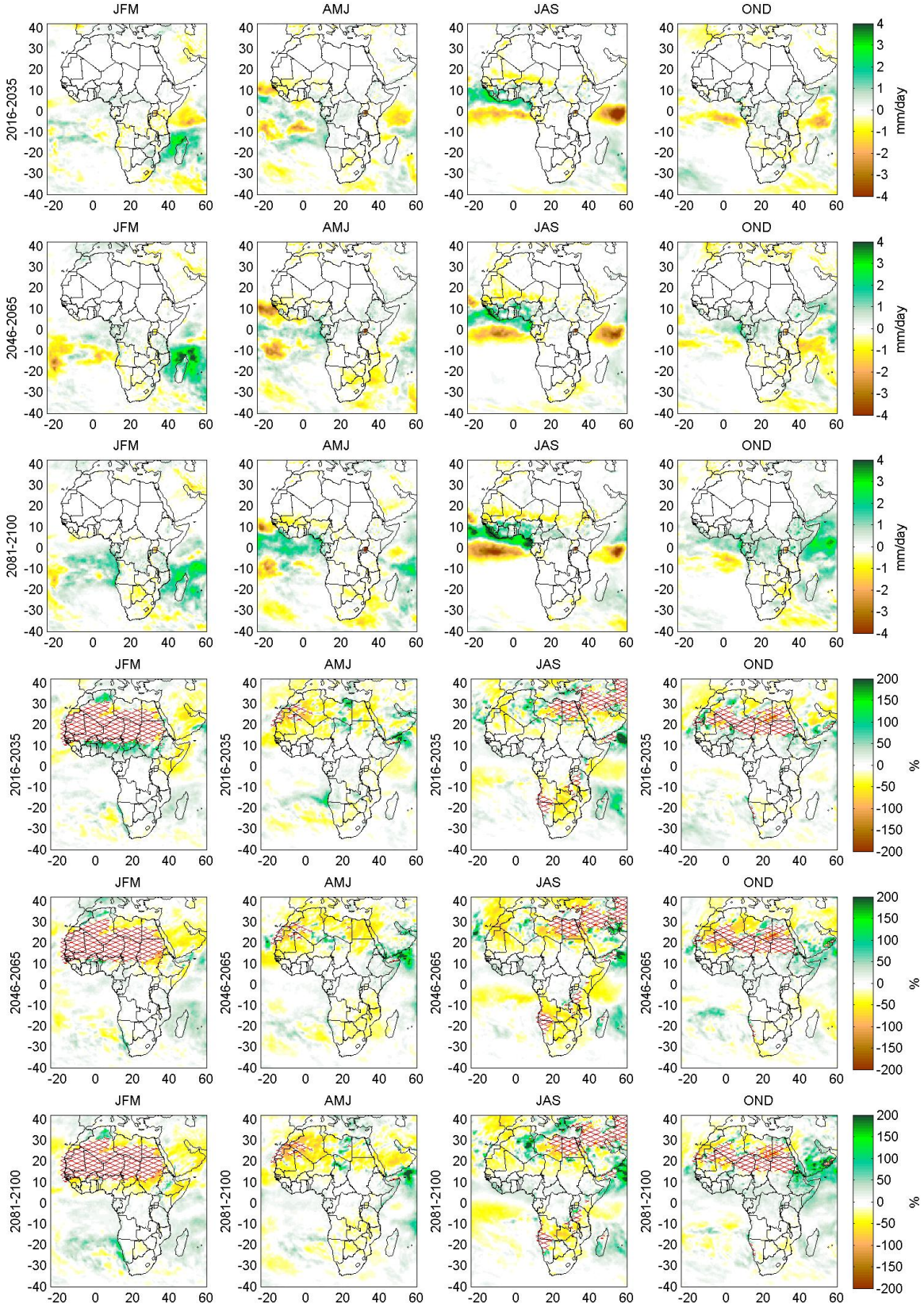

Figure 4.7: Projected change of seasonal mean precipitation according to RCP4.5 for three different future time-slices (2016-2035, 2046-2065 and 2081-2100) compared to the baseline time-slice 1986-2005. The three upper rows show absolute changes (in mm/day), while the three lower rows show relative changes (in %); in the latter plots areas where the absolute precipitation in the baseline time-slice is less that 0.05 mm/day have been hatched with red.

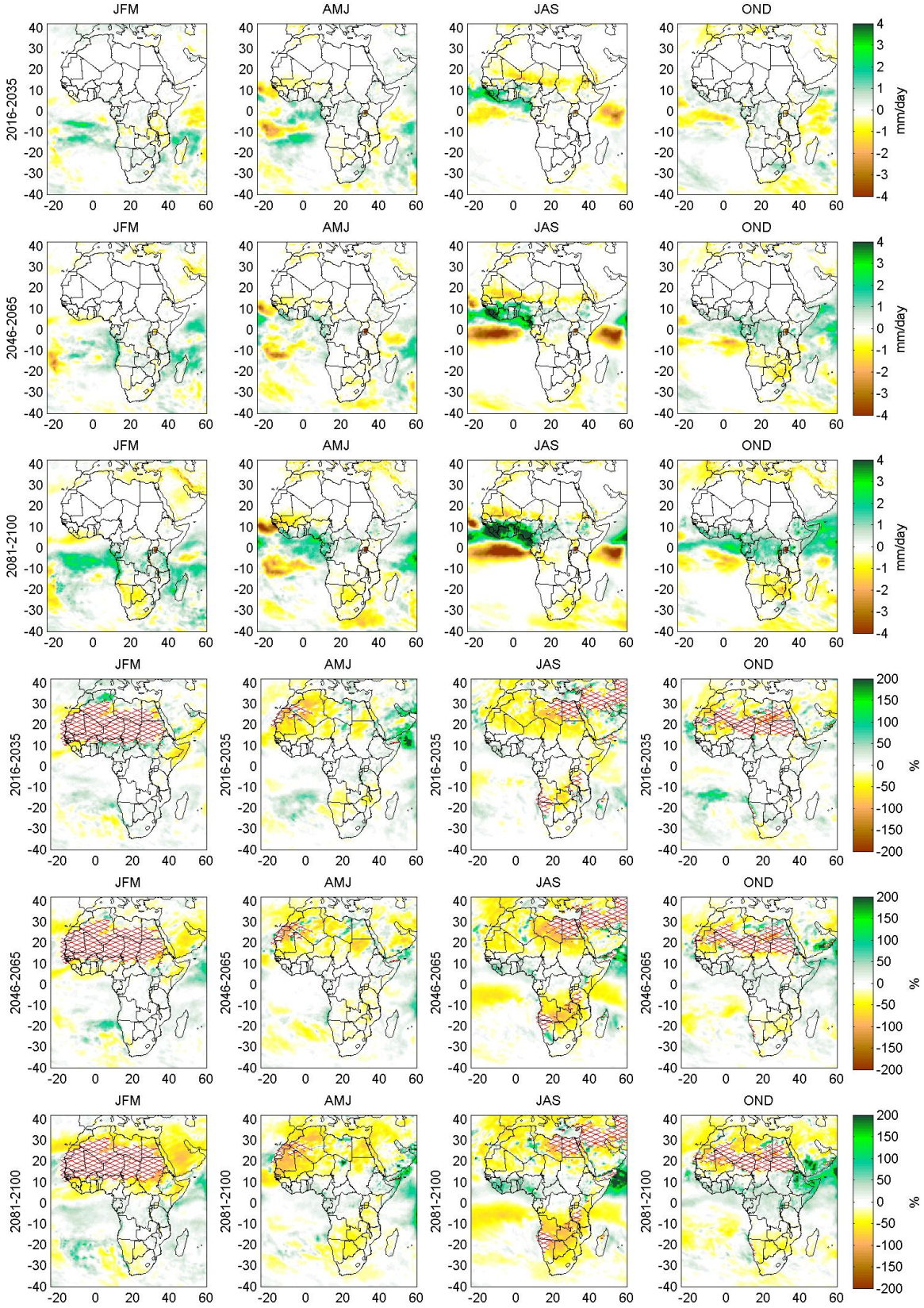

Figure 4.8: Projected change of seasonal mean precipitation according to RCP8.5 for three different future time-slices (2016-2035, 2046-2065 and 2081-2100) compared to the baseline time-slice 1986-2005. The three upper rows show absolute changes (in mm/day), while the three lower rows show relative changes (in %); in the latter plots areas where the absolute precipitation in the baseline time-slice is less that 0.05 mm/day have been hatched with red.

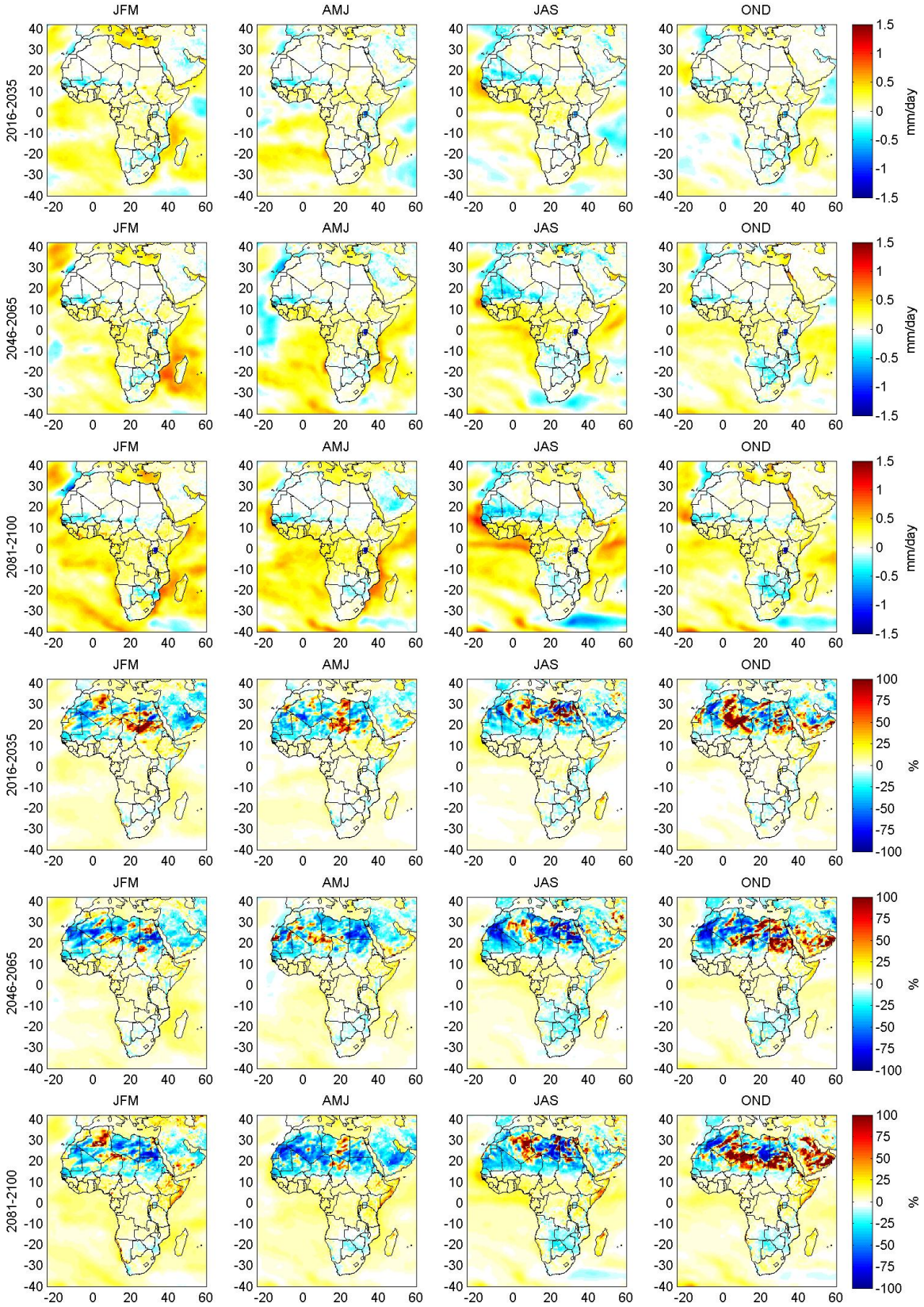

Figure 4.9: Projected change of seasonal mean evaporation according to RCP4.5 for three different future time-slices (2016-2035, 2046-2065 and 2081-2100) compared to the baseline time-slice 1986-2005. The three upper rows show absolute changes (in mm/day), while the three lower rows show relative changes (in %).

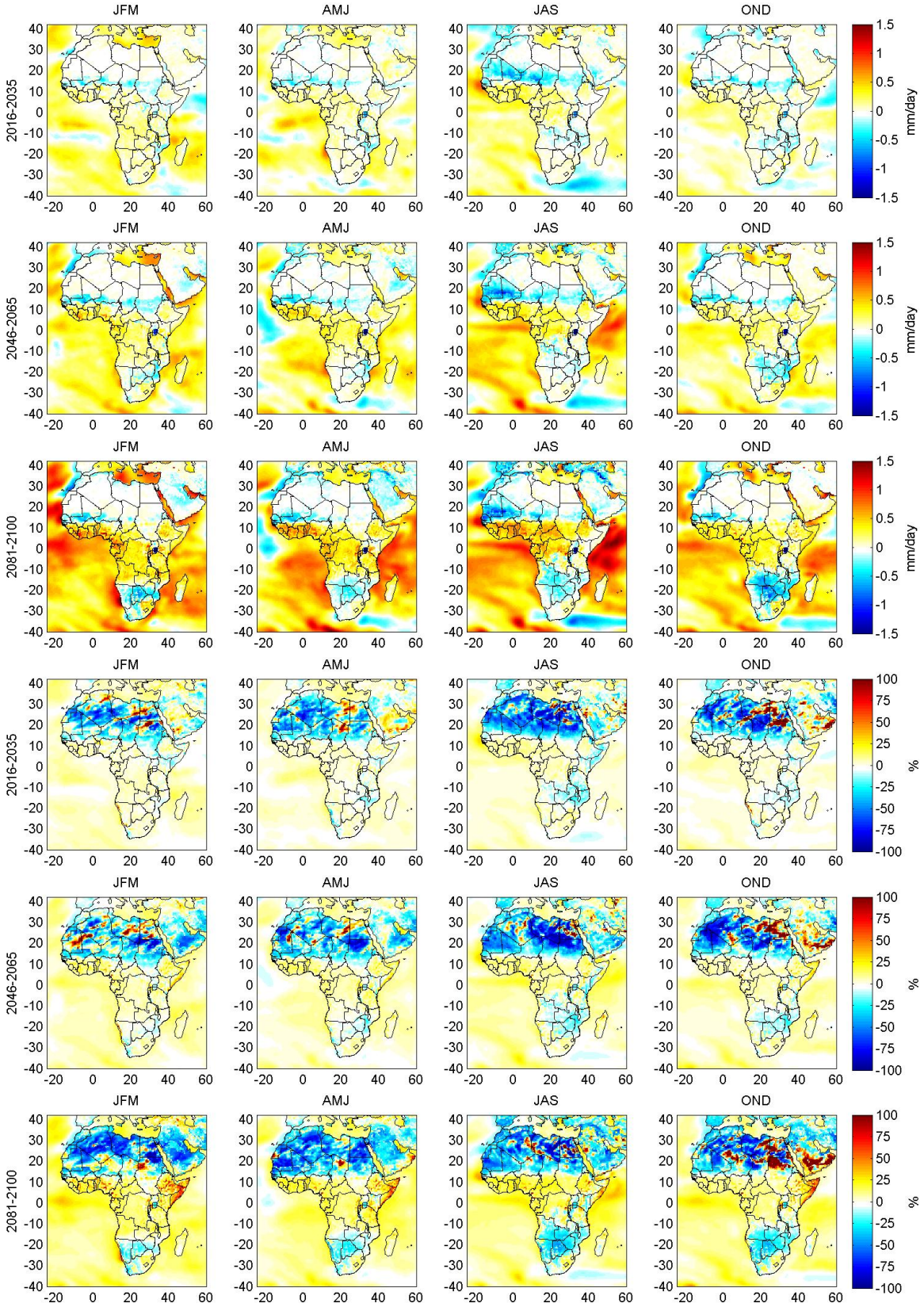

Figure 4.10: Projected change of seasonal mean evaporation according to RCP8.5 for three different future time-slices (2016-2035, 2046-2065 and 2081-2100) compared to the baseline time-slice 1986-2005. The three upper rows show absolute changes (in mm/day), while the three lower rows show relative changes (in %).

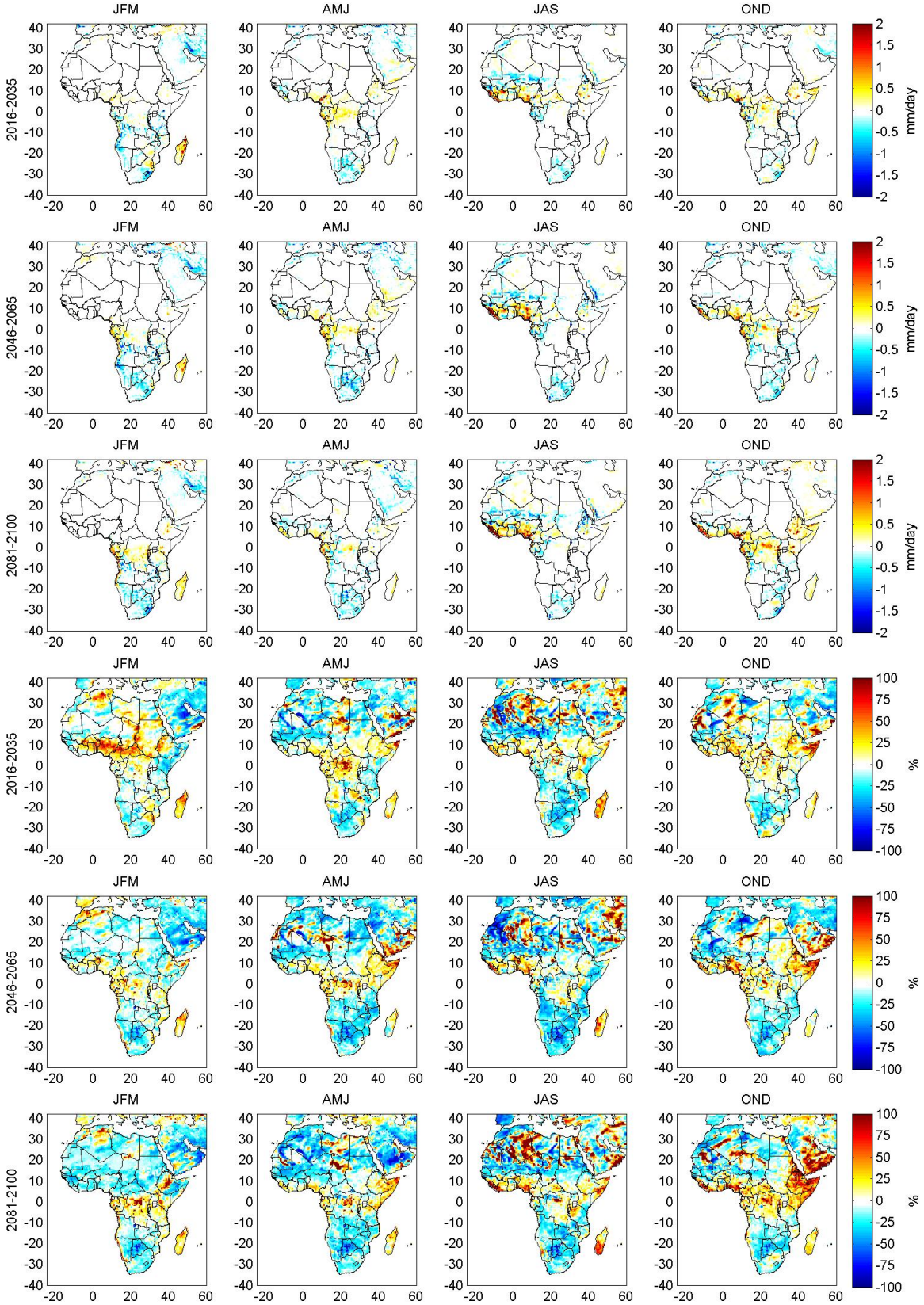

Figure 4.11: Projected change of seasonal mean total runoff according to RCP4.5 for three different future time-slices (2016-2035, 2046-2065 and 2081-2100) compared to the baseline time-slice 1986-2005. The three upper rows show absolute changes in mm/day, while the three lower rows show relative changes in %.

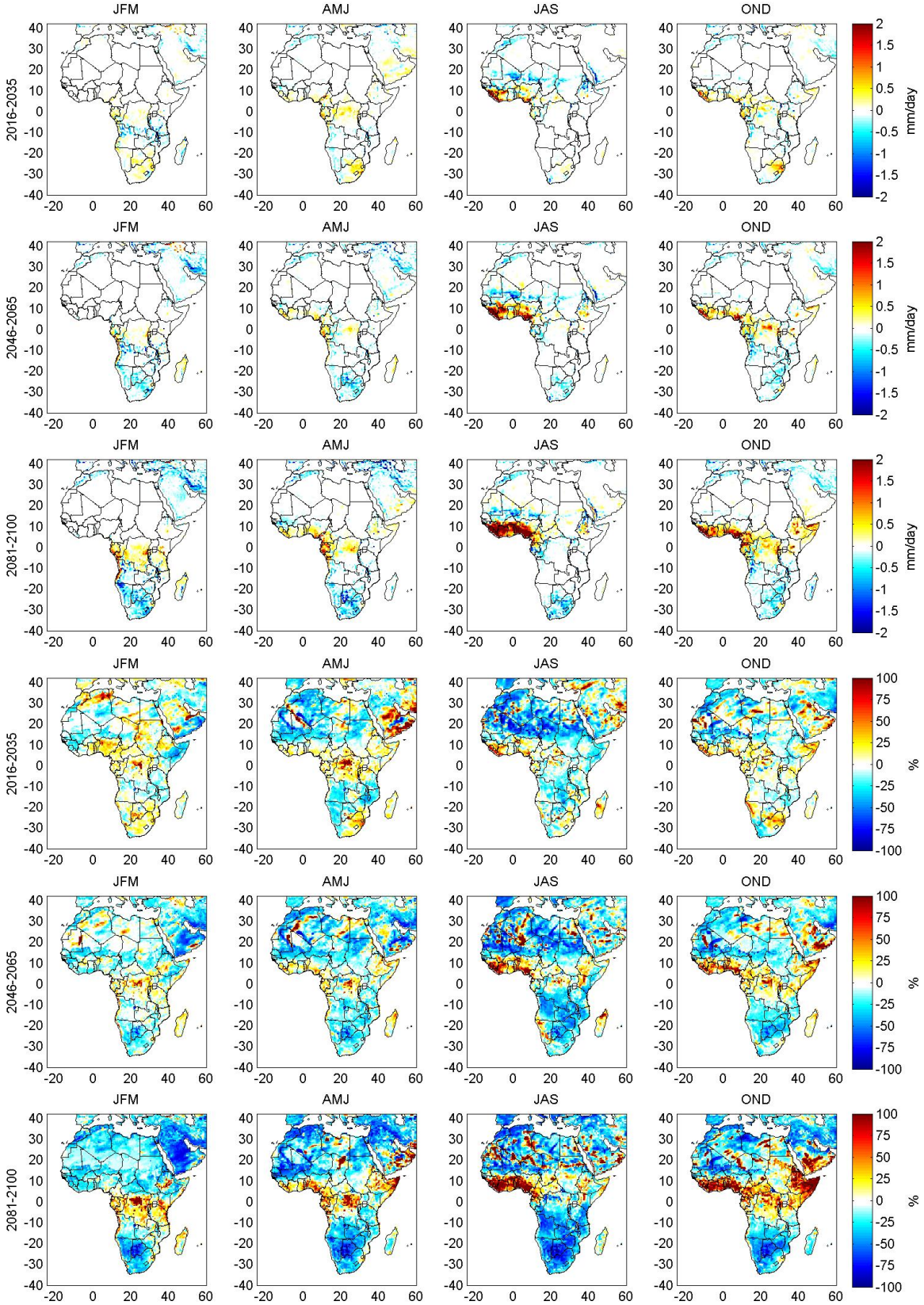

Figure 4.12: Projected change of seasonal mean total runoff according to RCP8.5 for three different future time-slices (2016-2035, 2046-2065 and 2081-2100) compared to the baseline time-slice 1986-2005. The three upper rows show absolute changes in mm/day, while the three lower rows show relative changes in %.

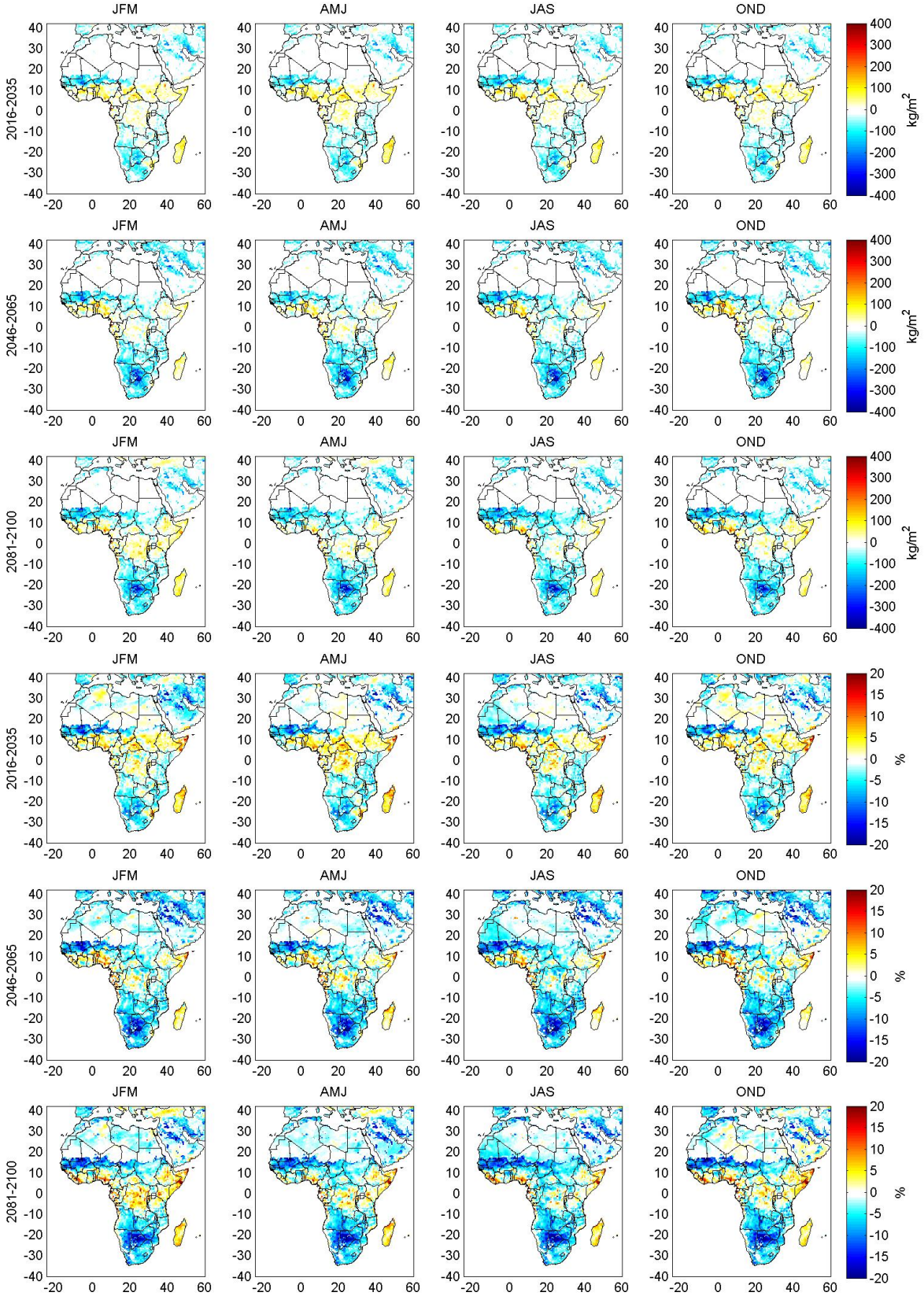

Figure 4.13: Projected change of seasonal mean total soil moisture content according to RCP4.5 for three different future time-slices (2016-2035, 2046-2065 and 2081-2100) compared to the baseline time-slice 1986-2005. The three upper rows show absolute changes in kg/m^2, while the three lower rows show relative changes in %.

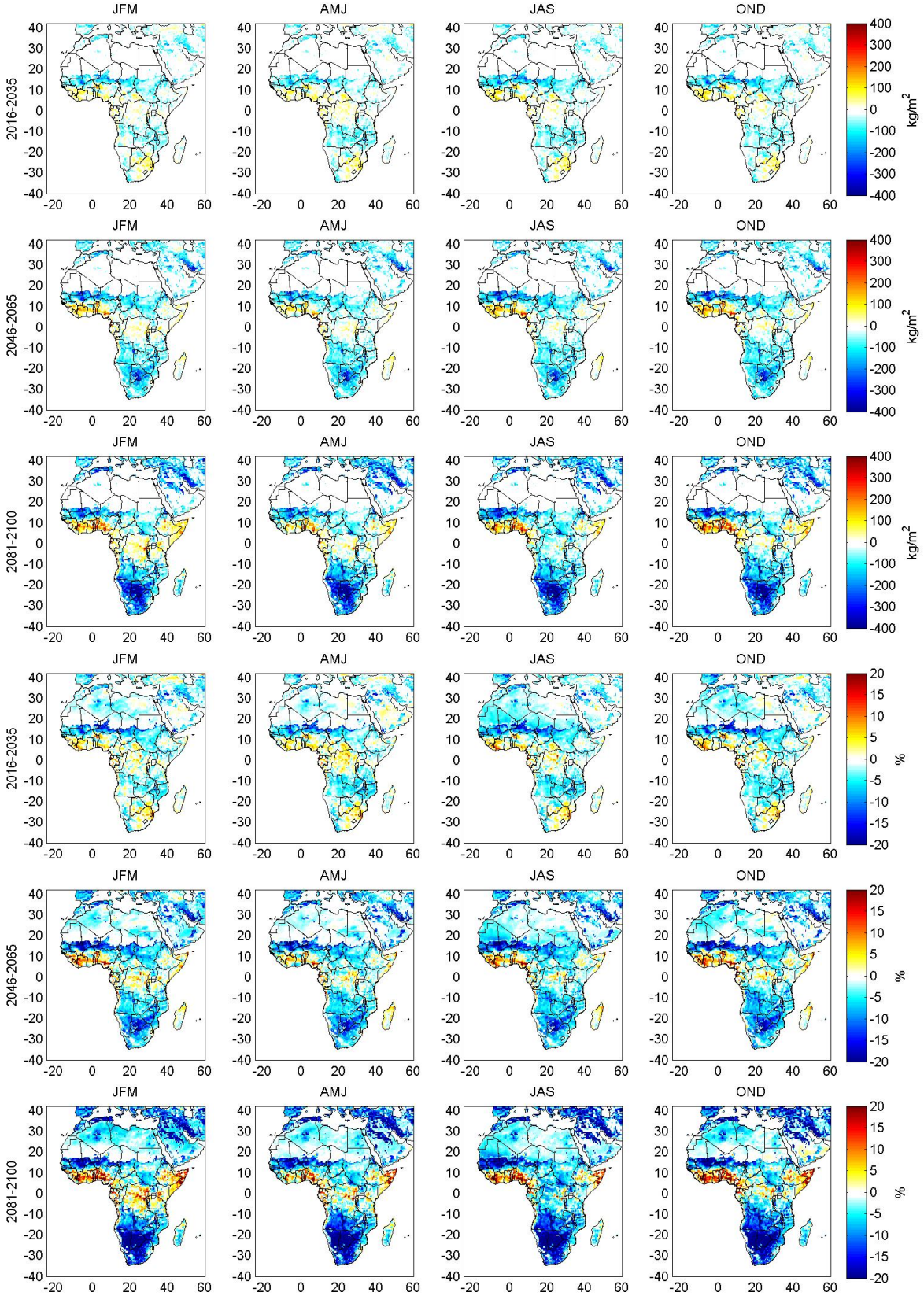

Figure 4.14: Projected change of seasonal mean total soil moisture content according to RCP8.5 for three different future time-slices (2016-2035, 2046-2065 and 2081-2100) compared to the baseline time-slice 1986-2005. The three upper rows show absolute changes in kg/m^2, while the three lower rows show relative changes in %.

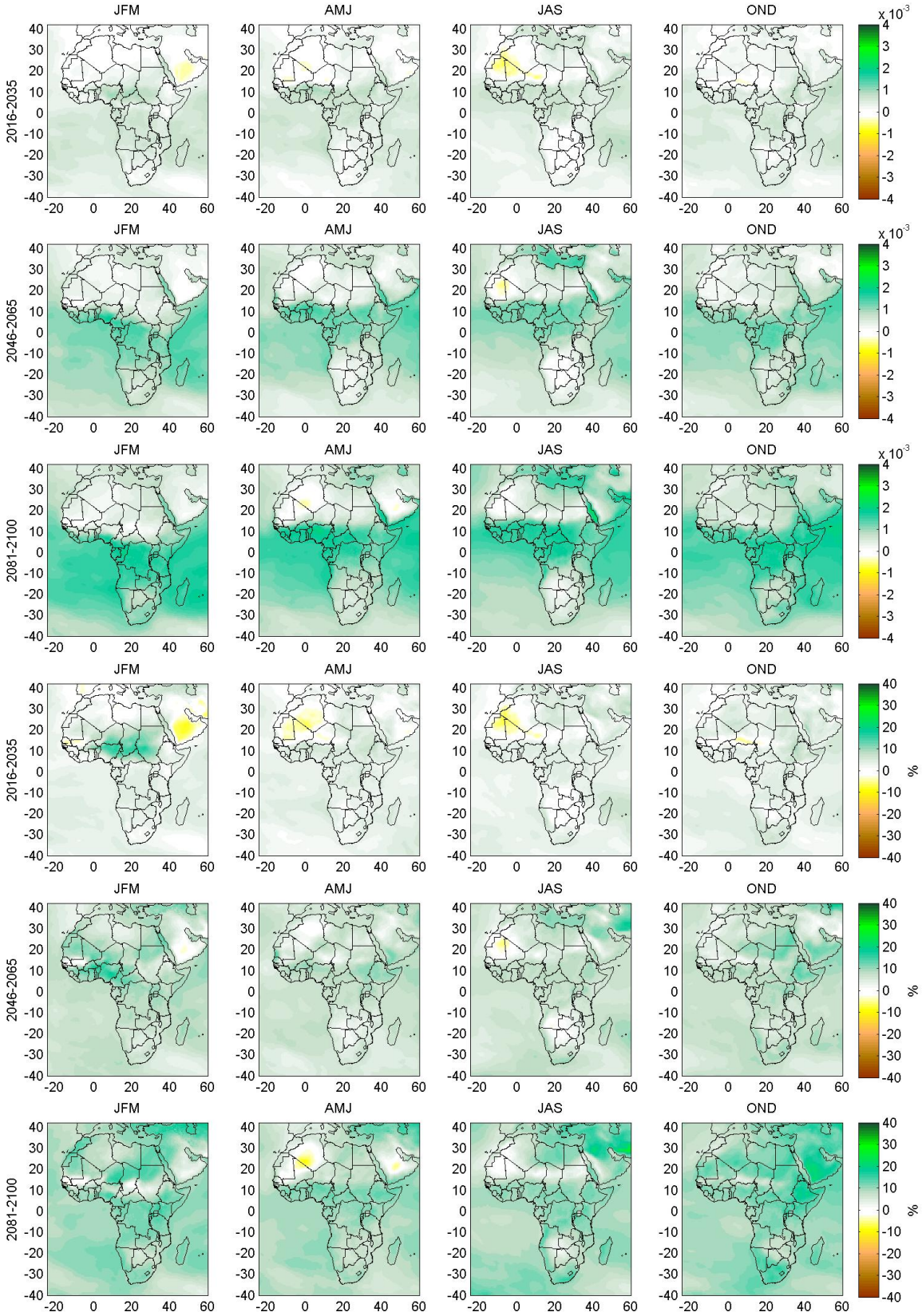

Figure 4.15: Projected change of seasonal mean specific humidity according to RCP4.5 for three different future time-slices (2016-2035, 2046-2065 and 2081-2100) compared to the baseline time-slice 1986-2005. The three upper rows show absolute changes, while the three lower rows show relative changes (in %).

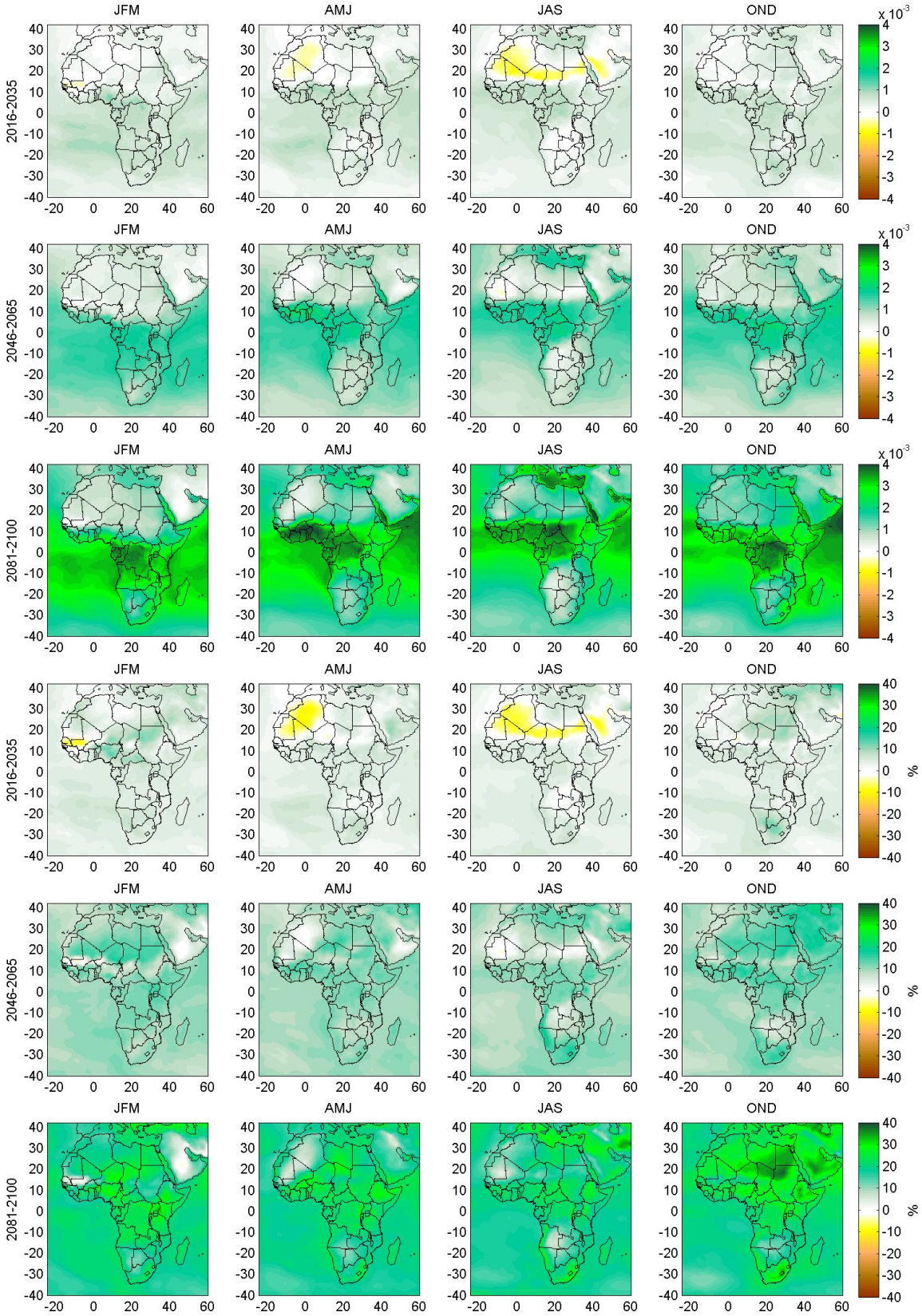

Figure 4.16: Projected change of seasonal mean specific humidity according to RCP8.5 for three different future time-slices (2016-2035, 2046-2065 and 2081-2100) compared to the baseline time-slice 1986-2005. The three upper rows show absolute changes, while the three lower rows show relative changes (in %).

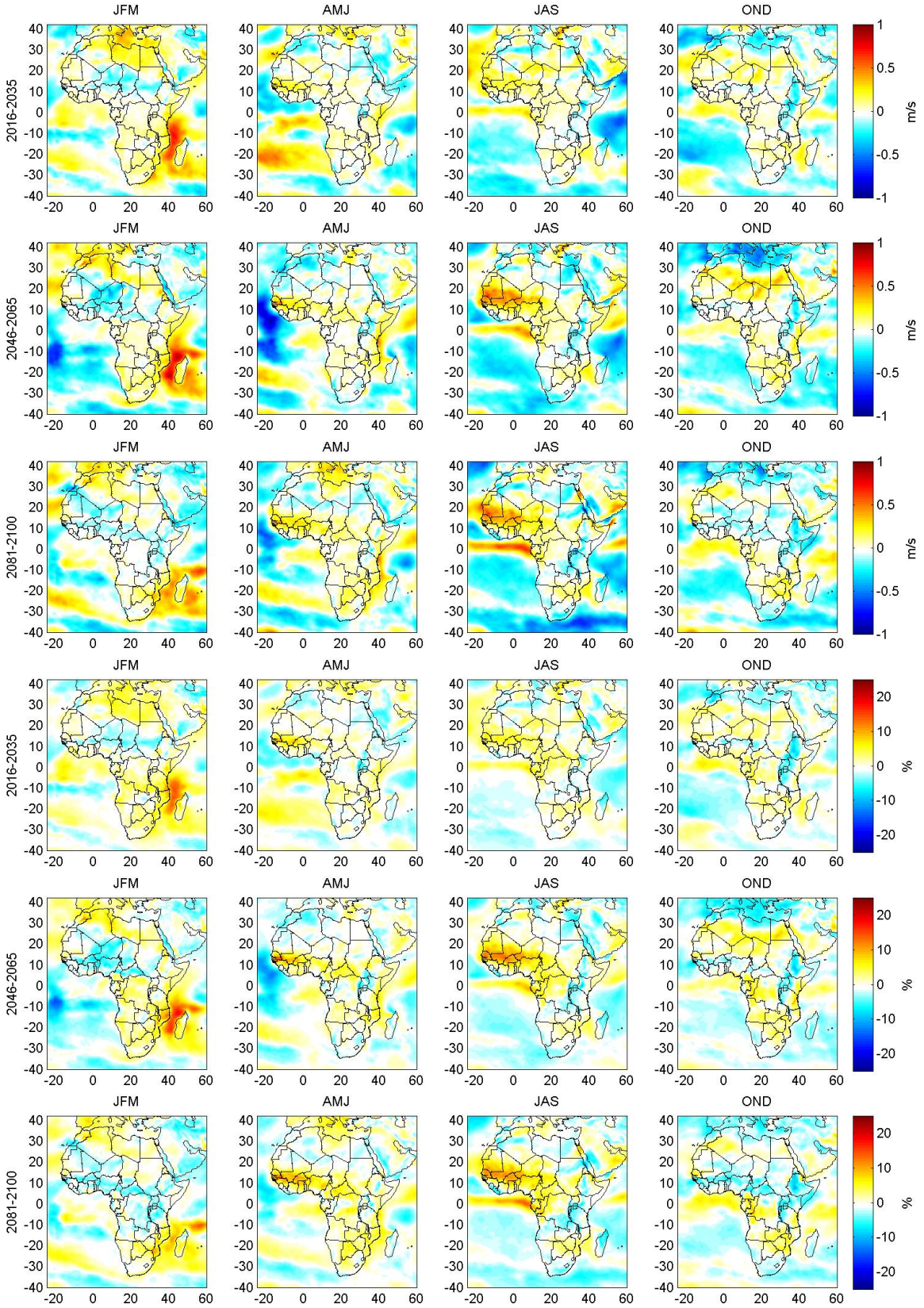

Figure 4.17: Projected change of seasonal mean surface wind speed (at 10m) according to RCP4.5 for three different future time-slices (2016-2035, 2046-2065 and 2081-2100) compared to the baseline time-slice 1986-2005. The three upper rows show absolute changes (in m/s), while the three lower rows show relative changes (in %).

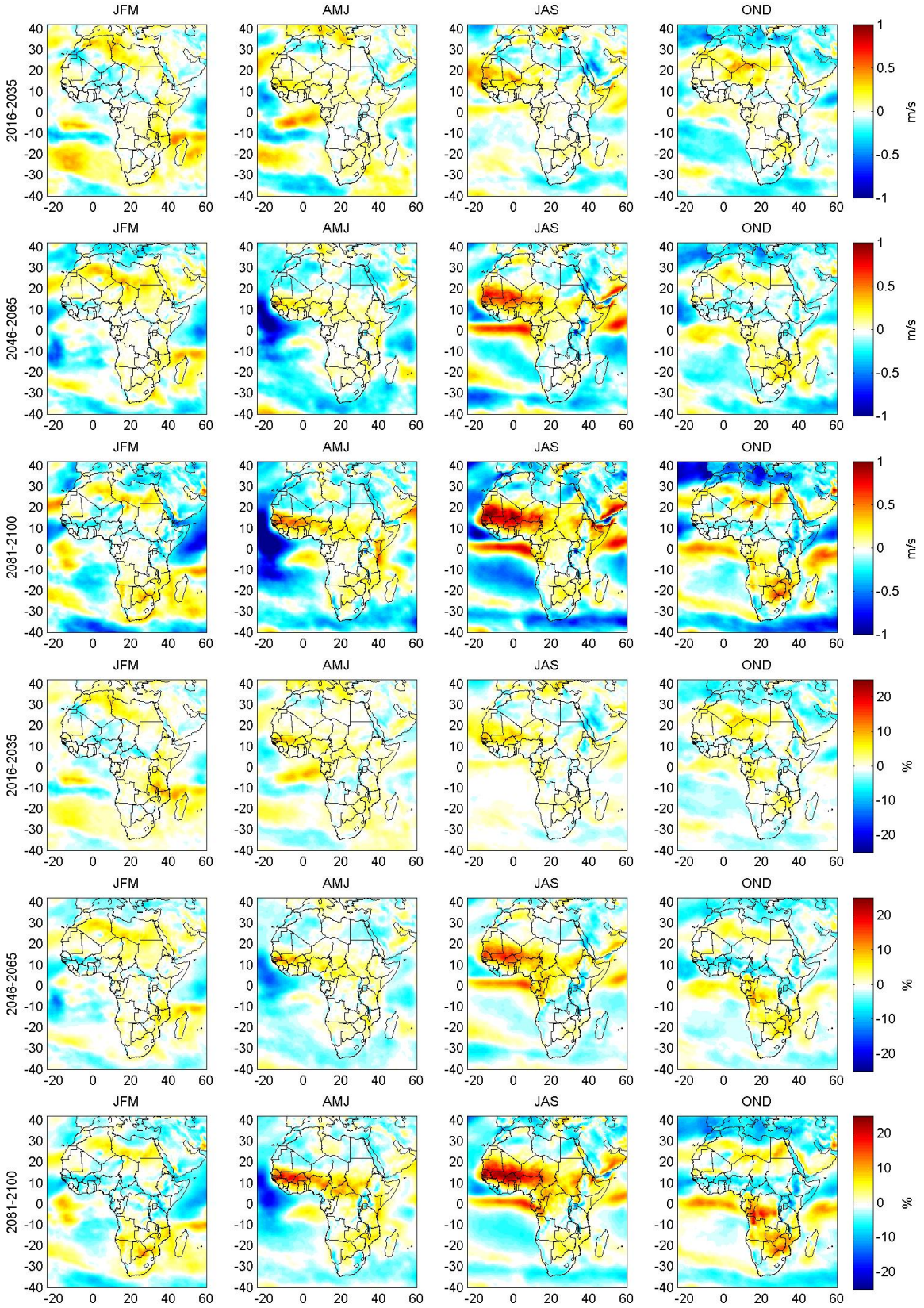

Figure 4.18: Projected change of seasonal mean surface wind speed (at 10m) according to RCP8.5 for three different future time-slices (2016-2035, 2046-2065 and 2081-2100) compared to the baseline time-slice 1986-2005. The three upper rows show absolute changes (in m/s), while the three lower rows show relative changes (in %).

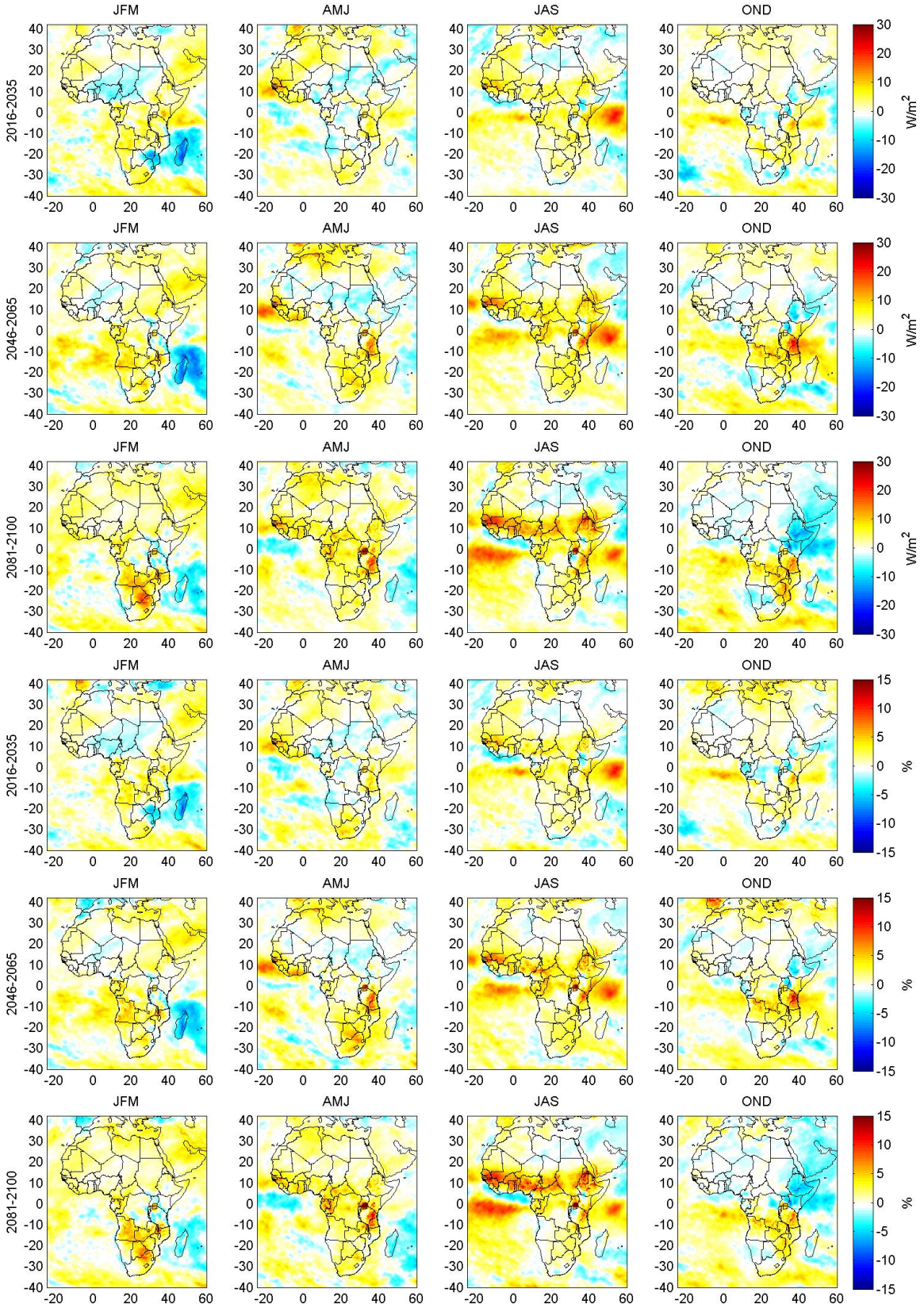

Figure 4.19: Projected change of seasonal mean shortwave downwelling radiation at the surface according to RCP4.5 for three different future time-slices (2016-2035, 2046-2065 and 2081-2100) compared to the baseline time-slice 1986-2005. The three upper rows show absolute changes (in W/m^2), while the three lower rows show relative changes (in %).

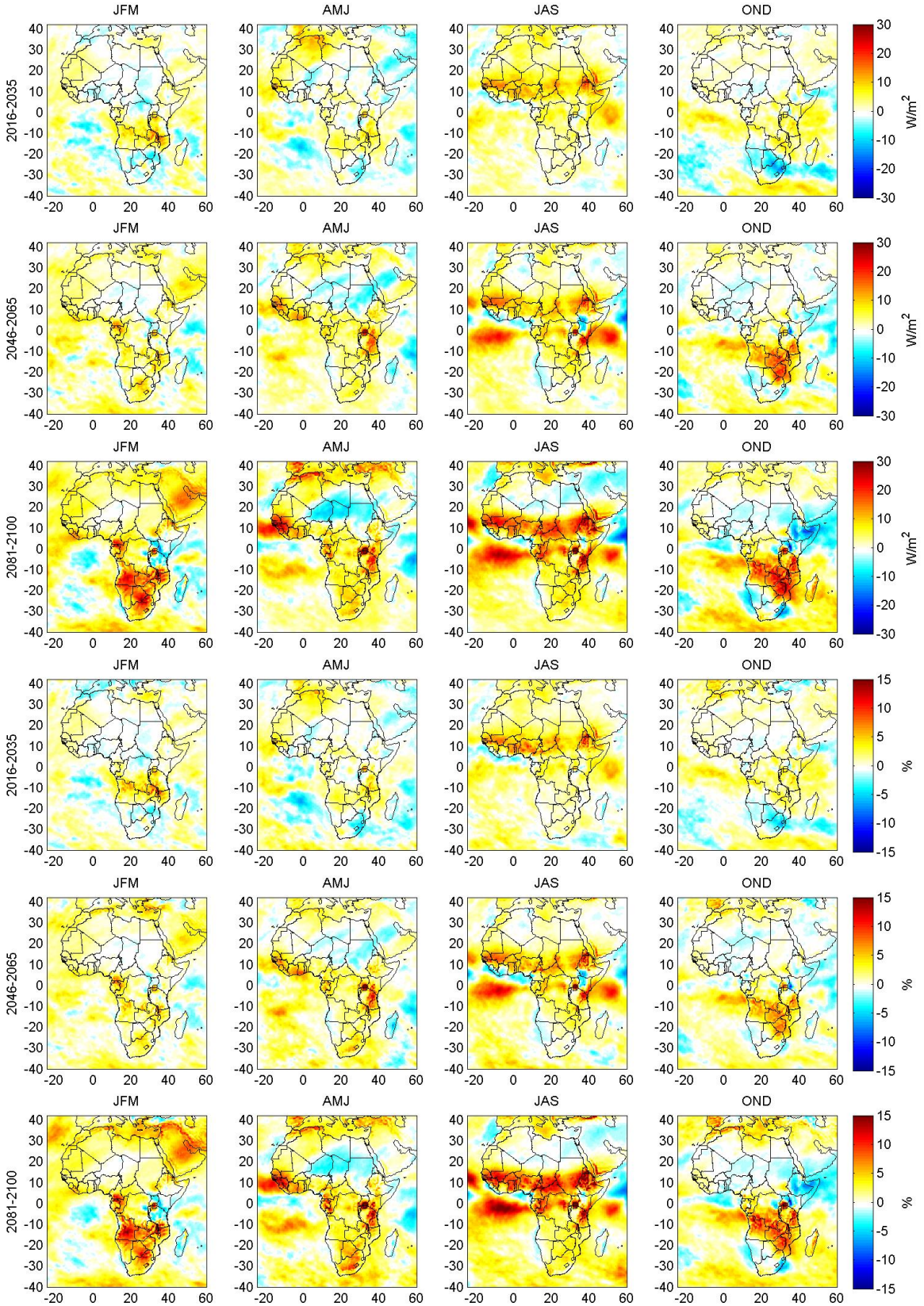

Figure 4.20: Projected change of seasonal mean shortwave downwelling radiation at the surface according to RCP8.5 for three different future time-slices (2016-2035, 2046-2065 and 2081-2100) compared to the baseline time-slice 1986-2005. The three upper rows show absolute changes (in W/m^2), while the three lower rows show relative changes (in %).

References

Christensen, O.B., Drews, M., Christensen, J.H., Dethloff, K., Ketelsen, K., Hebestadt, I., & Rinke, A., 2006. The HIRHAM regional climate model version 5 (β). DMI Technical Report 06-17, http://www.dmi.dk/fileadmin/Rapporter/TR/tr06-17.pdf.

Dee, D.P., Uppala, S.M., Simmons, A.J., Berrisford, P., Poli, P., Kobayashi, S., Andrae, U., Balmaseda, G. Balsamo, G., Bauer, P., Bechtold, P., Beljaars, A.C.M., van de Berg, L., Bidlot, J., bormann, N., Delsol, C., Dragani, R., Fuentes, M., Geer, A.J., Haimberger, L., Healy, S.B., Hersbach, H., Hólm, E.V., Isaksen, L., Kållberg, P., Köhler, M., Matricardi, M., McNally, A.P., Monge-Sanz, B.M., Morcrette, J.-J., Park, B.-K., Peubey, C., de Rosnay, P., Tavolato, C., Thépaut, N., & Vitart, F., 2011. The ERA-Interim reanalysis: configuration and performance of the data assimilation system, *Quarterly journal of the Royal Meteorological Society*, **137**, 656, 553-597.

Hazeleger, W., Wang, X., Severijns, C., Ştefănescu, S., Bintanja, R., Sterl, A., Wyser, K., Semmler, T., Yang, S., van den Hurk, B., van Noije, T., van der Linden, E., & K. van der Wiel, 2012. EC-Earth V2.2: description and validation of a new seamless Earth system prediction model. *Clim Dyn.*, **39**, 26112629, doi: 10.1007/s00382-011-1228-5.

Legates, D.R., & Willmott, C.J., 1990. Mean seasonal and spatial variability in gauge-corrected, global precipitation. *Int. J. Climatol.*, **10**, 111-127.

Matsuura. K., & Willmott, C.J., 2012a. Terrestrial Air Temperature: 1900-2010 Gridded Monthly Time Series, http://climate.geog.udel.edu/~climate/html_pages/Global2011/... README.GlobalTsT2011.html.

Matsuura. K., & Willmott, C.J., 2012b. Terrestrial precipitation: 1900-2010 Gridded Monthly Time Series, http://climate.geog.udel.edu/~climate/html_pages/Global2011/... Precip_revised_3.02/README.GlobalTsP2011.html.

Nikulin, G., Jones, C., Giorgi, F., Asrar, G., Buchner, M., Cerezo-Mota, R., Christensen O.B., Deque, M., Fernandez, J., Hansler, A., Meijgaard, E.V., Samuelsson, P., Sylla, M.B. & Sushama, L., 2012. Precipitation climatology in an Ensemble of CORDEX-Africa Regional Climate Simulations, *J. Clim.*, **25**, 6057-6078.

Uppala, S., Kållberg, P., Simmons, A., Andrae, U., Da Costa Bechtold, V., Fiorino, M., Gibson, J., Haseler, J., Hernandez, A., Kelly, G., Li, X., Onogi, K., Saarinen, S., Sokka, N., Allan, R., Andersson, E., Arpe, K., Balmaseda, M., Beljaars, A., Van De Berg, L., Bidlot, J., Bormann, N., Caires, S., Chevallier, F., Dethof, A., Dragosavac, M., Fisher, M., Fuentes, M., Hagemann, S., Hólm, E., Hoskins, B., Isaksen, L., Janssen, P., Jenne, R., Mcnally, A., Mahfouf, J., Morcrette, J., Rayner, N., Saunders, R., Simon, P., Sterl, A., Trenberth, K., Untch, A., Vasiljevic, D., Viterbo, P., & Woollen, J., 2005. The ERA-40 re-analysis, *Q J R Meteorol Soc*, **131**(612):29613012. doi:10.1256/qj.04.176